Characterization of Coronary Arteries:
Correlating Mechanical Stiffness with Staining for in vivo Imaging

Vivian W Hou

A thesis
submitted in partial fulfillment
of the requirements for the degree of

Master of Science

University of Washington

2018

Committee:

Eric J Seibel, Chair

John L Petersen II

Matthew O'Donnell

Program Authorized to Offer Degree

Bioengineering

University of Washington

Abstract

Characterization of Coronary Arteries:
Correlating Mechanical Stiffness with Staining for in vivo Imaging

Vivian W. Hou

Chair of the Supervisory Committee:

Professor Eric. J. Seibel

Department of Mechanical Engineering

Widespread prevalence of cardiovascular disease (CVD) in the US is indisputable. Over 82.6 million adults (~30% of the US population) have been diagnosed with one or more forms of CVD. Coronary artery disease (CAD) is the most common form and constitutes nearly 50% of all cases. It remains the leading cause of death for individuals afflicted with CVD due to the critical role of the coronaries in myocardial function. In coronary arteries, the CAD manifests as a highly-active, immune-driven sequestration of lipids which eventually triggers calcification that is found in advanced CAD lesions. Calcification is thought to provide stability as an atheroprotective mechanism even though deposition results in gradual stenosis and angina. Unstable or 'vulnerable' lesions are characterized with very little calcium deposition, yet these lesions are thought to result in myocardial infarction. Vulnerable lesions are difficult to observe by traditional approaches and are differentiated by thin-cap fibroatheromas (TCFAs). TCFAs are large, eccentric, necrotized lipid cores that are contained within the arterial wall by a thin fibrotic cap. Vulnerable lesions do not occlude the lumen and are not evident under conventional, non-invasive imaging, thus monitoring their structural progression is paramount for improving clinical outcomes. Histopathology is the gold standard for assessing lesion grade through H&E and other more specific stains. These dyes are toxic which preclude their use in vivo interrogation. Several imaging

modalities have thus been developed in lieu of conventional histology to circumvent this limitation. One of which is the Scanning Fiber Endoscope (SFE). Pilot SFE investigations on cadaveric specimens and biomarkers between the Human Photonics Lab (HPL) and the Center for CardioVascular Innovation (CCVI) led to the exploration and application of Evan's blue as a contrast agent for fibrotic caps. Evan's blue is an FDA-approved compound and is typically employed as an in vivo blood tracer for Boolean assessment of cardiac leakage, or output. The chemical compound also demonstrates increased affinity for fibrous cap components and exhibits spectral characteristics that permit SFE fluorescence imaging. Evan's blue stains in a graded fashion reflecting fibrotic cap content. An increased fibrotic cap content is directly associated with an increase in mechanical stiffness. We therefore hypothesize that the optical intensity of Evan's blue correlates with the mechanically stiff properties of diseased coronary arteries to support SFE detection for in vivo assessment. To test our hypothesis, the experimental histology laboratory at the CCVI was tailored to process human and porcine coronary specimens. This included all the classical steps in pathology along with high resolution imaging for quantification. Procured human (n = 7) and porcine (n = 10) specimens were first tested in a custom-designed mechanical apparatus assembled at HPL prior to histology. In proximity to the contracting myocardium, coronaries experience a greater amount of longitudinal stress during physiological activity and when coronaries are diseased. The mechanical apparatus thus measured displacements within specimens when a load (20-200 g) was applied to the sample. Coronary arteries were isolated and segmented (normal: n = 20, diseased: n = 14), and lengths/diameters were precisely measured. Segments were then mounted on a machined probe for testing. Vessel segments were loaded several times (n = 5) for a given mass and the experiment was repeated at least 5-8 times for fresh and frozen groups for both normal and diseased coronary segments. A knot in the suture line attaching the specimen to the calibrated mass provided a fiducial marker for vessel displacement. High resolution, high-speed cameras acquired video recordings of knot displacements where optical data were processed, and analyzed using ImageJ and MATLAB code. Displacement vs. force and stress vs. strain plots were produced for all experiments. Fresh, healthy segments displaced 500 um more than diseased samples and spanned a range of 1.5-3.3x. Frozen, healthy segments displaced an average of 400 um less than fresh segments suggesting the presence of a freezing-induced artifact. Comparisons between human and porcine segments revealed similarities in

their displacements suggesting that porcine arteries can substitute for disease-free arteries during longitudinal uniaxial testing. Following mechanical characterization, coronary segments were processed into microscope slides for pathological evaluation. Sections (n > 10 slides/group) were stained (Verhoeff's Hematoxylin - elastin/calcification, Aniline Blue - collagen, Evan's Blue - fibrotic caps) and quantified via ImageJ to determine collagen-to-elastin (C/E) ratios and degree of Evan's Blue staining. Although diseased tissue segments displaced less than normal segments, stress-strain analyses and the resulting Young's modulus values did not confirm our hypothesis of an expected increase in stiffness. It is thought that the varying cross-sectional areas of diseased segments may have contributed to this effect as a diameters and hence cross-sectional areas between groups were different by nearly 3 fold.

CHAPTER 1: INTRODUCTION

1.1. CARDIOVASCULAR DISEASE (CVD)

Cardiovascular disease (CVD) is the leading cause of globally death, manifesting as a family of conditions that afflict various aspects of the circulatory system. Despite the widespread prevalence of CVD, morbidity and mortality distributions do not necessarily coincide as the epidemiology of these conditions are subject to a variety of factors including socioeconomic influences, access to healthcare, and other facets of cultural modernization. Formerly CVD was thought to be associated with higher income countries, as disposable income facilitated unhealthy lifestyle changes such as consumption of food for reasons outside of nutrition (ie. soda pop) and increases in physical inactivity (ie. sedentary lifestyle).

The INTERHEART study across 52 countries reveals that the bulk burden (>80%) of CVD actually lies with low and middle income countries. Despite ranking among the higher income countries, closer examination of CVD prevalence in the US reveals the same trends. According to NHANES data from 2011-2014, over 92 million Americans presented with at least one CVD. Of these 92 million over 90% of this population were associated with low income risk factors.

1.2. CORONARY ARTERY DISEASE (CAD) AND CORONARY HEART DISEASE (CHD)

The CVD family comprises a variety of conditions, however the most prevalent condition is coronary artery disease. Coronary artery disease (CAD) and coronary heart disease (CHD) are used interchangeably to discuss the development and progression of atherosclerosis in the coronary arteries of the heart.

1.2.1. Chronic Inflammation – Physiological Insult

Advances in molecular biology, microscopy, and computational power greatly improved the ability of researchers to evaluate molecular pathways in connection to physiological developments. In the 1980s, cardiovascular medicine underwent a paradigm shift by acknowledging the immunogenic processes that

drive atherosclerotic development, effectively reframing development in context of chronic inflammation. The effects of chronic inflammation are very much dependent on the individual. As a general description, chronic inflammation induces shifts in the native tissue and immune population and often results in positive and negative remodeling of the local architecture.

1.2.2. Low-Density Lipoprotein (LDL), Oxidative Stress, and Immune Recruitment

Atherosclerotic development is initiated from the endothelial surface and manifests as a protective response against excess low-density lipoprotein (LDL) in the bloodstream. The exact mechanisms by which chronic exposure to high LDL levels trigger inflammation vary. In one pathway, excess oxidized LDL has shown to induce apoptosis in endothelial cells. Initiation of apoptotic signaling will trigger cellular stress signaling pathways in neighboring cells.

Endothelial cells routinely express low levels of recruitment markers for various immune populations, most notably short-lived monocytes. Recruitment is suppressed under normal physiological conditions, it is only in the context of inflammation that overexpression of these markers results in the necessary avidity for activating contact. Upon activation, the monocyte extrasavates into the local tissue, undergoing differentiation into a long-lived macrophage. The roles of these resident macrophages vary however these cells have been shown to upregulate expression of LDL receptors, increasing their uptake and storage of LDL. Some have hypothesized that this is a defensive effort to remove the offending soluble LDL as studies have shown that a drop in LDL levels result in the resolution of these cells. Failure to resolve these early accumulations results in progression as additional immune cells are recruited and the local cell populations undergo expansion, apoptosis, and necrotic cycles.

The gradual accumulation of dead cellular material and protective scarring creates deposits that are termed atheromas, lesions, or plaques. The terms lesions and plaques are used to describe a variety of disease structure and in the cardiovascular field they are often used interchangeably. Post-mortem histology studies have revealed that lesion progression is not linear, cycles of progression and regression are specific to the individuals. Although many other conditions and disorders can arise during atherosclerotic progression, the

scope of this research primarily concerns atherosclerosis affects the perfusion network of the heart, as such it is important to briefly examine the two major afflictions of end stage patients.

1.2.3. Clinical Progression – Stable Angina

In most individuals, progression of the disease occurs gradually and in a stable fashion. As lipid is accumulated within the arterial wall it gradually becomes necrotic as the resident macrophages undergo apoptosis. This cellular debris is not adequately cleared due to the constellation of local inflammatory signaling and eventually gives rise to a necrotic core. Cellular expansion and fibrotic deposition pathways are activated, perhaps in an effort to prevent contact between the necrotic content and the luminal blood stream as the interaction would be catastrophically thrombotic. Gradual growth of the core accompanied by growth in the fibrous cap result in luminal intrusion. Blood flow through the lumen can be generally characterized by Poiseuille's law wherein a 50% loss of the diameter results in 16-fold increase in resistance to flow. Shear forces on the luminal surface amplified which elicits gradual compensatory expansion of the vessel in a mitigation effort. Over the span of decades, the vessel can become heavily burdened limiting its ability to compensate and resulting in a loss of perfusion and subsequently, stable angina.

1.2.4. Clinical Progression – Myocardial Infarction

Myocardial infarction (MI) results from the abrupt cessation of perfusion to a large region of myocardium. This is often the result of thrombotic formation in one or more coronary branches. A loss of luminal diameter naturally predisposes a vessel towards occlusion however it is now understood that stenosis alone cannot be a predictor for MI risk. A combination of angiographic and post-mortem studies revealed that lesions responsible for MI could exhibit less than 50% loss in luminal diameter. The new understanding places more emphasis on the morphology of lesions and how likely they are to contribute to thrombose formation. Exact linkages between lesion morphology and MI require further elucidation.

1.3. OVERVIEW OF CARDIOVASCULAR ANATOMY AND ELECTROPHYSIOLOGY

An overview of normal cardiovascular anatomy and physiology is useful in establishing how disease progression occurs and how the changes affect diagnosis and treatment.

1.3.1. Human Adult Systems Level Anatomy

The adult human heart is a four-chambered organ that resides to the slight left of the thoracic cavity and comprises part of the mediastinum. Other locally presents organs and structures include the lungs and trachea, thymus, esophagus, great vessels, and several key phrenic and cardiac nerves. The heart is oriented such that the apex of the points to the lower left and the great vessels interface in the superior portion. Several pericardial layers encase the heart providing mechanical support, protection, and lubrication for cardiac activity, as the contractile motion is nearly continuous from the fourth week in prenatal development until death. Proceeding from the exterior, the comprising layers are the fibrous pericardium, parietal pericardium, and visceral pericardium. The fibrous and parietal pericardium are effectively continuous with one another forming the outer layer of the housing sac which is anchored to surrounding fascia and the thoracic wall. The visceral pericardium is continuous with the heart itself, interfacing directly with the myocardium to form the epicardium. Pericardial fluid fills the space between these two layers reducing friction during cardiac motion.

Threading through the epicardium are the main coronary arteries and veins. The coronary arteries stem off the aortic root and quickly branch off into myocardium to form the perfusion network that feeds the myocardium. The innermost surface of the heart chambers is called the endocardium and comes into direct contact with blood during heart motion.

1.3.2. Blood Flow Through the Heart

Deoxygenated blood returns to the heart by way of the venous system. Vessels of increasing diameter collect returning blood from organ systems and converge towards the superior and inferior vena cava. Similarly, blood returning from myocardial perfusion is collected into cardiac veins which eventually merge

into the coronary sinus. These vessels finally interface at the right atrium, localizing the deoxygenated blood. Gas exchange is the next immediate goal. Right ventricular filling results from a combination of filling by ventricular relaxation and contraction by the right atrium. Backflow is inhibited by the closure of the tricuspid valve helping to ensure efficient movement of blood. Approximately 60ml of fluid moves from the right atria into the right ventricle during filling.

Following ventricular filling, contraction of the ventricles drives blood from the right ventricle through the semilunar pulmonary valve into the pulmonary trunk where the blood is distributed into the lungs for re-oxygenation at the alveolar level. Oxygenated blood is returned into the left atrium via the pulmonary veins. Similar to the right, a combination of contraction and ventricular relaxation drives the blood through the mitral valve into the left ventricle. Finally, contraction by the highly muscular left ventricle drives the blood through the aortic valve towards systemic perfusion. The openings of the coronary arteries sit within the aortic root just proximal to the aortic valve.

Cardiac output provides vital perfusion to all other organ systems. In addition to providing oxygenation, systemic circulation is responsible for nutrient exchange, heat transfer, and transport of cells and signaling molecules between organ systems. In order to produce adequate pressure for system circulation, highly coordinated depolarization

1.3.3. Coordinated Depolarization of the Heart

Initiation of the contractile wave begins in the sinoatrial (SA) node located in the right atrial wall near the interface of the superior vena cava. A population of nodal pacemaker cells spontaneously depolarization approximately 60-120 times per minute (~1-2Hz) in most humans at rest. How this spontaneity is achieved is not entirely understood; this pacemaker population does not rely upon autonomic stimulus though it is certainly subject to its influences. Once the pacemaker cells fire, the depolarizing wave travels through the right atrium causing it contract. The signal also stimulates left atrial contraction by way of Bachmann's bundle. Following atrial contraction, the depolarizing wave arrives at the atrioventricular (AV) node located in the interatrial septal wall.

Conduction through the AV node is delayed; this interval is integral as the ventricles must be allowed to fill adequately prior to their own contraction in order to efficiently move blood. Electrically downstream of the AV node is the bundle of His which extends down the interventricular wall to the apex where they interface with Purkinje fibers interwoven in the myocardium. As the final action, the depolarizing wave is conducted upwards away from the apex through the ventricular walls. This physical inversion of motion is necessary as in a standing human, ventricular filling is accomplished with in line gravity however ventricular contraction must oppose the gravitational field to move blood into systemic or pulmonary circulation. Repolarization quickly follows the depolarizing wave in anticipation of the next electrical cycle.

While the SA nodal cells are the primary pace makers, the AV node and ventricular walls also contain pacemaking cells that give rise to contractile motion in the absence of upstream stimulation. The resulting motion is generally not as effective in comparison to stimuli originating in the SA node.

1.3.4. Electrocardiogram: Visualization of the Electrical Cycle and Corresponding Contraction

An electrocardiogram (ECG/EKG) is the spatiotemporal measure of depolarizing and repolarizing waves as they travel through the heart. Electrodes placed at various sites across the body form variants of Einthoven's triangle. Voltage differences read between two physical points reflect the local electrical state in response to the stimuli.

When taken with respect to time these potential variations are referenced relative to a subject's electrical ground (usually a combination of limb leads) and are visualized as sinusoidal like deflections from a baseline. The net compilation of these traces across the heart produce the characteristic EKG signature. A common error is interchangeable use of the terms leads and electrodes: the term 'lead' refers to the voltage potential between two electrodes. This confusion tends to arise as non-clinical EKG systems tend to use only three electrodes and read across the three leads formed, resulting in casual interchange of the terms.

A minimum of three leads are required to produce the classical EKG signature; clinically performed EKGs often use twelve leads across ten electrodes while bedside EKGs for long term monitoring tend to use a modified three lead system. Commercially available EKG systems sample at a variety of rates. As an example commercially available external defibrillators fall in the range of 500Hz; this is well above the Nyquist criterion of 2X the phenomenon rate as heart rates tend to fall between 0-3Hz. Dedicated EKG systems often record the output on cardiography paper traveling at a rate of 25mm/s. Normal human EKG signatures span a wide array of morphologies however a discrete set of features remain constant as they correspond to specific events in the contractile cycle. These features are labeled as P, Q, R, S, T and sometimes U. Briefly, atrial contraction is signified by the P-wave, ventricular contraction is primarily signified by the QRS complex, and finally repolarization by the T-wave. During normal cardiac function the atria depolarize first followed by a delay before ventricular depolarization. This temporal delay is reflected in the length of the PR segment. The U wave is seldom visible in healthy patients only becoming prominent during physiologic imbalances such as hypokalemia. Normal heart function, and more importantly abnormal heart function can be evaluated by examining the EKG output.

1.3.5. Abnormal Electrical Cycles and Defibrillation

Efficient cardiac function is a function of coordinated contraction and relaxation driven by electrical stimuli. Aberrations or deviations in stimulation and conduction result in arrhythmias that are often reflected within EKG readings. In some patients, the SA node fails to engage resulting in the AV node becoming the primary pacemaker. An EKG reading of these patients will reflect the lack of atrial contraction with a missing P-wave. The ability of an EKG to provide a real-time evaluation of electrical activity specific to regions of the heart makes it critical in the detection and evaluation of acute cardiovascular events such as myocardial infarction.

Aberrations in the electrical stimulus can result in a loss of coordination resulting in a quivering motion. Initially, the myocardium is still contracting but is often doing so out of sync. Akin to hitting a swing off resonance, the heart chambers can not muster the net strength needed to efficiently move blood. Clinically, this quivering of the chambers is called fibrillation and can be broadly split into atrial and ventricular

fibrillation depending on the afflicted chambers. Ventricular fibrillation can present as ST-segment elevation suggesting some failure to repolarize.

A common misconception is that a defibrillator shock ‘restarts’ the heart implying some cessation of electrical activity during MI. Rather than ‘restarting’ the heart, a more apt description is ‘resetting’ the heart; a defibrillator discharge drives an electrical impulse (emphasis on the short duration) through the conductive path in an effort to force depolarization. In cases where the SA node remains viable, forced depolarization may afford the node an opportunity to initiate coordinated stimulus.

As with all ischemic events, time is a critical factor. A quivering heart is highly inefficient at all perfusion, including delivery of blood to the itself. Prolonged loss of perfusion results in extensive infarction and loss of viability at critical pacemaker sites; in these events no amount of defibrillation can restore the native spontaneity this often results in patient mortality. This emphasis on timing underscores the importance of early diagnosis and real-time monitoring during the treatment process.

1.4. CORONARY PERFUSION OF THE MYOCARDIUM – ANATOMY PHYSIOLOGY

The heart is a highly metabolic organ and requires extensive perfusion. Despite transporting blood through its chambers, diffusion limits render the mere presence of oxygenated blood insufficient. As such, the heart the metabolic demands of the heart are met by dense vascularization fed from three major coronary arteries originating directly from the aorta. It is no accident that the coronary ostia are located just proximal of the aortic valve; the heart supplies itself before any other organ.

The two major ostia give rise to the right and left coronary branches so named for their general directional courses. The right coronary artery (RCA) wraps around to the right following the atrioventricular (AV) groove until it reaches the posterior side of the heart. The left main coronary artery (LMCA) quickly bifurcates into the left anterior descending (LAD) and left circumflex (LCX or LCA). The LAD proceeds down the anterior

of the heart towards the apex. The LCX, like the RCA continues to follow the AV groove to the left until it reaches the posterior.

Exact branching and perfusion patterns vary greatly between patients however some insight into clinical challenges associated with treatment can be gleaned by examining anatomical trends. Clinical studies reveal that in 60% of patients, the RCA gives rise to the SA nodal artery with the LCX giving rise to the other 40%. The AV nodal artery is supplied by the RCA in 80% of patients. Similarly, upon reach the posterior, either the RCA or LCX can give rise to the posterior descending artery (PDA). In 70% of angiographic studies this is the RCA, while the remainder arise from the LCX or more uncommonly, exhibit co-dominance in which both RCA and LCX turn downward and give rise to a network of smaller branches or even anastomose.

Given the majority of human hearts are 'right handed' and that major pacemaker sites are often perfused by the right, there exists a temptation to assume that the right portion of the heart is more critical. It is important to weigh other parameters, the LAD alone supplies 40-50% of the left ventricular myocardium with the other significant portion supplied by the LCX. Recall that final propulsion of blood into systemic circulation is highly-dependent upon efficient left ventricular performance.

1.5. NORMAL CORONARY ANATOMY AND HISTOLOGY

A brief examination of normal coronary anatomy is necessary to discuss disease progression as it is critical to understand the shifts in vessel composition and how these changes affect overall vessel behavior.

1.5.1. General Vessel Architecture

Arterial and venous architecture are reflective of their differing roles in the cardiovascular system, arteries carry blood away from the heart to other organs and with the exception of the cardiopulmonary interface (and the transiently present umbilical vein), contain oxygenated blood. In comparison to most veins, arteries are subjected to higher pressures that are necessary for systemic perfusion. To this end, their composition

tends to be more robust than their venous counter parts possessing thicker, more muscular walls. The vessel wall contains three major layers, the intima, the media, and the adventitia.

1.5.2. Tunica Intima

The inner lumen of blood vessels are lined with a tightly knit monolayer of squamous endothelial cells. Beneath this are the supporting layers for these endothelial cells including a network of collagen and fibroblasts. Finally, the intima boundary is specified by the internal elastic layer (IEL), an elastic layer providing crucial expansive and contractile properties.

1.5.3. Tunica Media

Where the intima could be considered an interfacial layer, the media is comprised of layered smooth muscle cells and elastic fibers. This medial layer confers mechanical elasticity to the vessel, allowing the vessel to expand and contract to accommodate the contractile drive from the heart. Larger arteries have more medial layers and the largest vessels are ringed with additional elastic lamina; in the coronaries there normally only one IEL.

1.5.4. Tunica Adventitia

The outermost layer of tissue that is histologically vessel, where the media provides flexibility the adventitia provides mechanical strength. Unlike the previous layers which are cell rich, the adventitia is primarily matrix substance most notably collagen and a few fibroblasts. The border between the media and adventitia is delineated by a second elastic layer termed the external elastic layer (EEL). Histologically, innervation for the media can be observed in the adventitia as the nerves do not directly usually synapse onto the media.

1.5. CORONARY ARTERY DISEASE HISTOLOGY

For course of this discussion, the author will be adopting the histological stages as proposed and defined by the current leaders in cardiac pathology. Conventional histology of the coronaries is performed cross-sectionally and reflects the view of vessels as conduits for blood transfer subjected to pulsatile flow.

Blood infusion from the aorta forces both radially and longitudinally. Loss of luminal diameter due to lesion encroachment results in increased shear stress on the vessel surface. The interplay of progression and regression in the context of dietary and lifestyle influences, personal genetics, aging, and medical treatment result in vastly different lesion morphologies. Conventional histology of coronary arteries can only be performed after tissue excision as it is not possible to biopsy the heart.

1.5.1. Intimal Thickening

Prolonged inflammatory stimulation elicits the clonal expansion of endothelial cells resulting in a 'thickening' of the intimal layer. This is considered the first step in lesion development even though intimal thickening alone is not considered pathologic and is not specific to atherosclerotic development as it has been observed in transient inflammatory responses (ie. bacterial infection). If the source of the inflammation is resolved then the intima will gradually revert to a monolayer, however in the context of chronic inflammation, intimal thickening continues as additional cell populations are recruited. Eventually, the forming lesion will begin to extend into the luminal wall, disrupting the IEL. IEL disruption is one of the first features in pathologic progression along with increased presence of lipid-laden macrophages (foam cells).

1.5.2. Fibroatheromas

The continued sequestration of lipid by foam cells results in their eventual apoptosis, releasing the cellular contents into the wall. This local accumulation of necrotic debris trigger additional distress pathways attracting even more immune cells and stimulating local expansion of cell lines associated with fibrotic deposition. Collagen and elastin deposition on the luminal surface creates a fibrous cap that can protrude into the lumen, obstructing blood flow. The collagen matrix deposited is structurally different in comparison to basement collagen (III, IV). Unlike elastin which is highly expansive, the fibrous cap components are highly constrictive and lead to a loss in motility in the regions where present. When it first develops fibrosis is highly local to the underlying lesion creating a mechanical disconnect in the vessel. This loss in expansive ability coupled with the additional flow stress experience due to luminal protrusion is one of the driving forces in further progression. Geometrically, the lesion begins to expand outward into the lumen causing a

reduction in diameter. At this stage, the plaque often increases its angular coverage proceeding expanding circumferentially. The edges of the forming lesion are actively remodeled in part due to breakdown of the native matrix by matrix metalloproteins (MMPs). Early fibrous lesions feature a cap overlying a well-defined lipid core, more advanced fibrous lesions may feature more complex, highly necrotic cores with cholesterol clefts, and even medial calcification.

1.5.3. Calcified Lesions

Similar to fibrotic deposition, calcification of lesions could be viewed as a protective response. Calcification tends to be located either intramurally or luminally. The luminal presentation, while occlusive to flow, is hypothesized to provide stabilizing reinforcement to lesion caps. In comparison, the mural development of calcification appears to contribute to plaque instability by further instigating mechanical disconnects between the lesion and remaining soft tissue.

1.5.4. Chronic Near and Total Occlusions

As a plaque grows in size, it begin to lower the luminal diameter (briefly talk about radius to the fourth) As a point of discussion, 50% loss of the initial luminal diameter is a clinical indicator for intervention. Occlusion need not be complete to create disturbances, any loss of adequate perfusion results in infarction. Angina or chest pain is the result of gradual occlusion leading to the increasing loss of perfusion. Occlusion can present more dramatically in the form of acute myocardial infarction (heart attack) in which some plaque events causes the formation of a clot resulting in the sudden and near complete occlusion of one or more coronary branches or arteries.

1.5.5. Vulnerable Lesions

The defining geometry and composition of vulnerable lesions has evolved since their initial conception. There are several main morphological features that are categorized as vulnerable. The first general morphology features a thin fibrous cap overlying a large necrotic lipid core. It is hypothesized that some acute mechanical trigger causes the fibrous cap to rupture allowing a sudden burst of necrotic content to

come into contact with blood flow. The bolus of necrotic content triggers the thrombotic pathway creating a large clot that leads to occlusion.

The second general morphology features a denuded fibrous cap which has lost its protective endothelial layer. Direct exposure of collagen and fibrin to the bloodstream can cause the formation of micro clots on the surface. It is hypothesized that the clots may either accumulate on the cap surface, growing in size and reducing lumen diameter until the pressure breaks off the clot or that the surface throws off miniature clots over time and eventually one of these miniature clots eventually setting up an acute MI event.

Plaque shoulders, the regions where lesions interface with the surrounding tissue, are of particular interest and hypothesized to be prospective rupture points. Tissue remodeling occurs at the shoulders of lesions suggesting these regions are less mechanically stable due to MMP action. During periods of rapid lesion progression, matrix degradation may outpace fibrotic deposition.

It should be noted that while the vulnerable lesion hypothesis is relatively well-embraced by the medical community, the mechanistic ties between structure, rupture, and ultimately MI remain to be elucidated. This understanding is limited in part by the ability to observe lesion behaviors *in vivo*, the following section highlights some of the current solutions to this obstacle.

1.6. PERCUTANEOUS CORONARY INTERVENTION

The first percutaneous coronary intervention (PCI) was officially performed in 1977 by Andreas Roland Grüntzig. PCI bridges the treatment space between non-invasive management (ie. medication, lifestyle shifts, etc.) and open-chest procedures (ie. coronary artery bypass graft (CABG), heart transplant, etc.) Although still invasive, relative to open-chest procedures the catheter approach considerably minimizes surgical trauma.

The major goals of PCI are to improve and restore flow in the coronary vessels and attempt to offset future occlusion events that could lead to myocardial infarction. Angiography remains the gold standard for guidance and diagnosis during catheter lab intervention. Use of a C-arm provides the desired angiographic view in the presence of intravenously administered contrast agents. Angiograms non-invasively assess and estimate degree of occlusion within the coronary arteries. Catheter entry occurs primarily from the Common Femoral Artery (CFA) although approach from the radial artery has gained popularity in recent years. The CFA approach maintains several advantages including larger diameter allowing the entry of larger interventional instruments. Since conception, the field has rapidly expanded and evolved to incorporate a wide range of adjunct devices. PCI procedures fall into two major classes, angioplasty and atherectomy.

Balloon angioplasty refers to a set of procedures where a deflated balloon is delivered to site of narrowing within a vessel. The balloon is then inflated and effectively reopens the vessel by forcibly crushing the lesions outwards into the wall. Stents are often deployed at the site to ensure the vessel remains open. These stents are usually nitinol (nickel-titanium alloy) and may elute drugs that discourage restenosis. Restenosis in stents is a complex issue wherein the native vessel responds to the presence of the stent resulting in pathologic proliferation. Part of this response may be due to the mechanical disconnect between the relatively stiff nitinol stent and surrounding soft vessel tissue.

Atherectomy refers to procedures involving the use of a rotating burr to bore through highly occluded regions. The majority of atherectomy procedures primarily target regions of heavy calcification and occlusion as the burr is designed to minimally affect soft tissue. Laser atherectomy employs the use of a pulsed, cold laser to remove the obstructing material, this particular variant encountered setbacks when it was found that the laser pulses produced violent perturbations in routinely used contrast mediums.

1.7. CATHETHER-BASED IMAGING MODALITIES

PCI remains interventional at this time however the development of catheter-based imaging modalities has provided avenues for quickly gathering diagnostic information. Angiography provides a bird’s eye view for

procedural guidance however it is only able to elucidate larger, radiopaque features. The majority of plaque components (ie. fibrosis, necrotic lipid etc.) are radiolucent. The coronary arteries cannot be biopsied meaning there is no way of providing conventional histologic analysis for these regions while the tissue remains in the patient. To meet this need, catheter imaging modalities have been developed to provide a form of 'virtual' histology. By employing light and sound, these modalities can resolve the desired lesion details and provide the opportunity to observe the lesion more carefully during intervention. Many of these modalities have been commercialized and some are routinely applied during catheter lab procedures. This discussion aims to briefly compare these modalities and frame the interventional space they occupy.

1.7.1. Intravascular Ultrasound (IVUS)

Intravascular ultrasound (IVUS) is a side-scanning modality that pulses acoustic waves in the 10-40MHz range from the catheter tip. The waves travel into the tissue and echo back differentially depending on the material properties of the tissue components it encounters. Harder substances, such as calcification, are highly echogenic, in contrast softer components such as the normal media are less echogenic, and do not return the acoustic waves as efficiently.

As the IVUS tip rotates, it emits acoustic waves and collects the resulting echoes, this information is reconstituted into a tomographic view of the vessel wall at the tip location. Hyperechoic regions are visually rendered as white to reflect higher signal intensity, hypoechoic regions are dark to represent a lack of return. IVUS is the clinically established standard for catheter imaging and is routinely applied to assess lesions during intervention. IVUS excels at identification of dense tissue materials and has the added advantage of thorough wall penetration ranging between 4-8mm. In comparison to light based modalities, IVUS is only minimally affected by the presence of blood and does not require 'clearing' of the vessel prior to imaging.

1.7.2. Intravascular Optical Coherence Tomography (IVOCT)

Intravascular Optical Coherence Tomography (IVOCT) employs near-infrared light (1300nm) to side scan the vessel wall. Images are formed in a manner similar to IVUS however in this case the modality is light, use of light results in loss of wall penetration depth (1-2mm) due to scattering however greatly improves

the imaging resolution. IVUS typically resolves features in the range of 100-150μm whereas IVOCT can resolve features in the range of 10-20μm, an almost 10-fold improvement. In comparison to IVUS, IVOCT can provide a high-resolution view of the vessel inner surface including key features such as calcified nodule and stent struts. Unlike IVUS, IVOCT imaging is greatly attenuated by the presence of blood, a contrast flush must performed in order for proper operation, limiting its clinical applicability.

1.7.3. Intracoronary Near-Infrared Spectroscopy (NIRS)

Intracoronary near-infrared spectroscopy (NIRS) is another major side-scanning effort to employ near-infrared light in order to identify features of interest in atheromas. In contrast to IVOCT systems, NIRS uses a range of near-infrared light spanning from 800-2500nm in order to produce a spectral response across the range. Lesion components exhibit different spectral responses, as such the NIRS system produces chemograms and aims to further characterize the biochemical composition of the lesion components rather than focusing solely on structural characteristics. The penetration depth of NIRS is similar to that of IVOCT and is ultimately limited by the shortest wavelengths it uses (800nm), relegating its penetration depth to approximately 1mm.

1.8. THE SCANNING FIBER ENDOSCOPE (SFE)

In comparison to other endoscopes, the Scanning Fiber Endoscope (SFE) is ultrathin and flexible at 1.2-1.6mm in diameter, well suited to minimally-invasive applications. In comparison with conventional angioscopes, it is similar in size range and in field of view (~70º), however unlike conventional scopes the SFE is able to deliver high resolution images and can be modified to perform both reflectance and fluorescence imaging. Other research endeavors have already implemented the SFE for in-vivo imaging including in the bile duct, fallopian tubes, and in the carotid arteries.

1.8.1. Resonance and Piezoelectric Fiber Scanning

Mechanical excitation of an optical fiber at its resonant frequency gives rise to the large sweeping motion that the SFE relies upon to achieve light delivery across a relatively large field. Image formation is reliant

upon correlation between fiber position and returned optical data. Near-field diffraction facilitates rejection of out-of-focus light, resulting in the production of high-resolution images. Fiber position is governed by resonant excitation and braking, tighter control of both can be achieved by carefully parsing out the resonant frequency during catheter calibration and subsequent use. The spiral scanning pattern is used by most SFE related research endeavors, to achieve the spiral pattern the piezoelectric tube housing the fiber provides stimulation in two orthogonal axes in an exponentially decaying sinusoidal fashion.

1.8.2. Color Splitting and Multimodal Lasers

SFE research systems are equipped with a wide range of lasers. Some systems are purely RGB-based (~444nm, ~532nm, ~635nm) and some systems feature additional specialized wavelengths (405nm, 488nm, 785nm etc.) White-light reflectance imaging is the primary application of the SFE however the system is designed in such a fashion that individual lasers and channels can be controlled. This is accomplished in part through software control via custom LabVIEW modules, but also through hardware design. The color splitting system uses a system of dichroic filters and mirrors to separate wavelengths prior to PMT acquisition. Software control allows assignment of values read from the PMT to specific color outputs (not unlike color assignment in confocal imaging). The combination of laser control and PMT control allows the system to easily switch between reflectance and fluorescence imaging. In some systems, the two can be performed simultaneously.

1.8.3. The Scanning Fiber Endoscope for Angioscopy

For application in the coronary arteries, the SFE posses some notable advantages. As a forward-viewing system, it can provide guidance in an intuitive fashion interventional navigation. Guide wire delivery is the cornerstone of percutaneous coronary interventions. The complex variations in coronary path and heavy occlusion can hinder delivery of guidewires as these obstacles are difficult to visualize under conventional angiography. In addition to providing guidance for procedures, the concurrent fluorescence and reflectance capabilities of the SFE system place it in an optimal position to perform molecular imaging. Application of fluorescently bound probes specific for disease may provide additional information regarding coronary behavior in-vivo. Pilot work performed in the coronaries reveal that under RGB

reflectance imaging, the coronary surface remains shades of pale pink and yellow, with no discernible discoloration associated with lesion presence. Translation of the SFE for lesion assessment will require the identification of a suitable contrast agent.

1.9. TOWARDS LESION VISUALIZATION IN THE CORONARY ARTERIES

Coronary occlusion can give rise to a myocardial infarction, however the discrete mechanisms by which this process occurs are unclear. It is well-accepted that vessels with heavy disease burden are at greater risk given their inherent loss in luminal diameter. The vulnerable lesion hypothesis states that certain morphological characteristics predispose a lesion towards rupture and subsequent clot generation, the features however, remain under contention.

1.9.1. Fibrous Caps and Evans Blue (EvB)

Early pilot immunofluorescence work was performed on coronary tissue in an effort to identify cell surface biomarkers associated with lesion presence. This endeavor was confounded by tissue limitations as the primary source was cadaveric, resulting in the degradation of these markers.

While a fresh tissue pathway was pursued, literature searches revealed a more robust candidate contrast agent, Evans Blue (EvB). EvB is FDA approved for intravenous administration and has been previously used to measure cardiac output in a manner similar to measurements made with indocyanine green and fluorescein. EvB demonstrates affinity for albumin amongst other serum proteins. Some research efforts also revealed an affinity for the fibrous caps of atheromas. As a final advantage, the dye spectral characteristics align with the SFE system parameters; under RGB examination the dye is a deep blue however it also fluoresces in the deep red following green excitation. As fibrous caps become more extensive during disease progression, successful identification of fibrous caps on the luminal surface represents an avenue into diagnostics.

1.9.2. Specific Affinity of EvB for Fibrous Cap Components

Although literature and early pilot work showed some affinity of EvB for fibrous caps, it is unclear exactly which lesion components are favored. There existed the temptation to perform a purely histologic study to examining EvB staining on cadaveric tissue. Following dye perfusion in saline, subsequent histology could be correlated to EvB stain intensity. Blood pharmokinetics are complex, simple application of the dye to cadaveric tissue would not adequately recapitulate the environment found *in vivo.* As a result, it would difficult to assess the relationship between staining intensity and disease progression. Instead, another measurand for disease progression was needed. Fibrotic deposition has been shown to be mechanically stiffer in comparison to healthy segments, as such a measure of vessel stiffness was proposed as the linkage between lesion progression and EvB staining of fibrotic caps.

1.10. TISSUE BIOMECHANICS – MEASURANDS AND METHODS FOR INTERROGATION

Mechanical interrogation can reveal properties of the tissue that explain its behavior *in vivo* and comparisons between healthy and diseased states can help elucidate the mechanisms that give rise to chronic and acute cardiovascular events.

1.10.1 Young's Modulus (E)

Young's modulus (E), sometimes referred to as the elastic modulus, concerns the deformation of tissue in response to opposing forces applied along axes. Formally, it is justified as a ratio of shear and strain and typically bears the units of pressure (N/mm^2):

$$\boldsymbol{E} \equiv \frac{stress}{strain} = \frac{\sigma}{\varepsilon} = \frac{\vec{F}/A}{\Delta l / L_0}$$

Assessment of Young's modulus is usually performed on a small scale to better localize the elasticity. If an artery is placed into a Cartesian system and we allow the z-axis to represent the longitudinal axis down the lumen then evaluation quickly yields that coronary vessels are isotropic with respect to x and y. We would

expect that interrogation of these different axes would reveal different elastic moduli. To this end, pursuing uniaxial assessment of coronary arteries is a practicality.

1.10.2. Tension and Distension During the Cardiac Cycle

Section 1.3 provided an overview of the cardiac cycle. As the heart contracts, the overall twisting motion can be described as a double knot. The main branches of the coronary arteries travel epicardially and are subjected to this overall contractile force (most notably the LAD). The major body of published literature focuses upon the radial and circumferential mechanical response of vessels to pulsatile blood flow. In this work, we proposed to further investigate the properties of coronary arteries in response to longitudinal forces.

1.17 HYPOTHESIS.

Briefly: Generally, disease progression results in an increase in fibrotic content, particularly in the luminal cap. An increase in fibrotic content should result in an increase in stiffness. Pilot work performed on Evans Blue demonstrates some affinity for fibrotic cap contents.

We propose that Evans Blue can be used as a surrogate marker for evaluating mechanical stiffness and define the following two hypotheses:

Hypothesis 1: Diseased arteries have increased stiffness in comparison to normal arteries

Hypothesis 2: Evans Blue staining intensity will be higher in more diseased, stiffer vessels in comparison to normal arteries

CHAPTER 2: METHODS

The methods presented in this chapter represent only a subset of the techniques and designs applied in the overall research endeavor to draw comparisons between catheter-based imaging modalities, conventional histology, and mechanical measurements. The specific methods detailed in this thesis reflect a concerted effort to mechanically characterize tissue and perform subsequent histological analysis.

2.1. TISSUE PROCUREMENT

Great consideration must be given to specimen sourcing, transport, and storage when the downstream intention is to assess optical, mechanical, and molecular properties. The crux of this thesis work and the overall research effort in turn, are heavily reliant upon tissue state. To this end, we begin our discussion with a consideration of the samples used for this investigatory work.

2.1.1. Heart Procurement – Porcine Frozen

Structural similarity to the human heart makes porcine hearts an apt substitute for human samples. In accordance with University restrictions, fresh frozen porcine hearts were procured from approved in-state abattoirs (Kapowsin Meats Inc., Graham, WA; Pure Country Pork, Ephrata, WA). Animals were routinely sacrificed at approximately 6mo in alignment with the company practices; hearts are procured at the time of processing by the abattoir staff in accordance with research protocols approved by the University of Washington.

Efforts were made to acquire the samples fresh from the source however physical distance from the procurement site made timely acquisition challenging. Despite hearts being procured the morning of, tissue degradation was evident during subsequent histology due to unavoidable time delays between harvest and sample reception. To this end, in order to maintain sample integrity, hearts were frozen at the procurement site then shipped to the University. Samples were then thawed overnight in saline at 4°C for next-day use or placed into storage at -20°C.

2.1.2. Heart Procurement – Porcine Unfrozen

Ice formation in tissue results in a number of artifacts that affect properties including mechanical stiffness and cellular degradation. To overcome freezing and degradation challenges, an on-site source of porcine hearts was sought out. This led to the acquisition of hearts from a University of Washington based research group (Applied Physics Laboratory (APL), Seattle, WA; Center for Industrial and Medical Ultrasound (CIMU), Seattle, WA) focused upon lithotripsy in the bladders of otherwise healthy pigs. Average time between sacrifice and sample reception did not exceed an hour in comparison to the 6-8hrs expended in the abattoir pathway. Immediate access allowed further implementation of tissue sustaining protocols such as immersion and partial perfusion using cold, anticoagulant (acid-citrate-dextrose) saline solution which improved overall experimental outcomes.

2.1.3. Heart Procurement – Human Cadaveric Frozen

Donor cadaveric hearts were procured from several non-transplant, national research and education donor networks (MEDCURE, LSA, SW, etc.) Drawing from the greater pool of cadaveric tissue greatly expands the array of conditions seen in the tissue and improves the population representation of the resulting data. As a general protocol, organ procurement is performed by the donor network; samples can be requested based upon given parameters (ie. serology, age, sex, etc.).

2.1.4. Heart Procurement – Human Explant Unfrozen

Fresh, unfrozen human hearts were obtained through an organ procurement option via a non-transplant donor network based within the greater Washington-Alaska-Montana-Idaho (WAMI) region. Due to possible HIPAA concerns the specific procurement details cannot be discussed however all samples arrive with accompanying serology.

2.2. DISSECTION AND EXTRACTION OF CORONARY VESSELS FROM INTACT HEARTS FOR MECHANICAL TESTING

All samples were processed with utmost caution regardless of species origin and serology; great care was taken to minimize possible aerosolizing of fluid. Frozen samples were thawed from -20°C overnight in saline at 4°C. Prior to processing, samples were rinsed in room temperature saline and housed in a room temperature bath in-between dissection steps (< 1hr). Photos were acquired of the anterior and posterior view of the heart to determine general physical metrics. The aorta and pulmonary trunk were then removed to reveal the coronary ostia and reduce obstructing structures.

2.2.1. Porcine Coronary Extraction

Coronary extraction in porcine samples is straightforward, use of curved-blade Metzenbaum's results in easy separation of the vessel from the surrounding tissue planes. Following identification of the ostia, the primary coronary trunks are located upon the epicardial surface. Using the concomitant veins as a natural separation plane, the epicardium is gradually peeled back to reveal the main coronary paths. Under gross visual observation, forceps are used to provide tension as the coronaries are lifted and excised from the epicardium. Major branches are collected at this stage to preclude accidental nicking of the main vessel. Following general excision, grossing is performed by carefully trimming side branches to lengths <1mm. Epicardial fat and excess connective tissue are removed from the adventitial surface.

2.2.2. Human Coronary Extraction

In human samples, coronary paths show more variation and heavy fibrosis and calcification confound connectivity. The presence of epicardial fat is more pervasive in human samples in comparison to porcine samples. As such, tactile feedback is critical in determining exact coronary path and in ascertaining general attachments to surrounding connective tissue. Following initial visualization of the coronary ostia, tactile feedback is used to carefully remove the epicardial tissue from the adventitial surface. Unlike porcine extraction, use of the concomitant vein does not always guarantee avoidance of the main vessel.

As such, the main coronary is trimmed at the ostial site and forceps are used to provide tension on the coronary as the epicardium housing the vessel is separated from the heart surface. A back-lit dissection pad is used to enhance contrast as the coronary is carefully excised from the surrounding tissue. Attachment of epicardial fat is far more tenacious in human samples, demanding laborious excision from the surrounding connective tissue. Great care must be given not to remove the adventitia as the presence of adipose tissue it is more difficult to parse out the adventitial plane.

2.2.3. Sample Segmentation and Determination of Disease Status

Following excision, both human and porcine coronaries are housed in cold saline baths to slow degradation and prevent desiccation. Photos and measurements are taken to ascertain general vessel dimensions and morphologies.

Prior to segmentation, vessels are removed and gently blotted dry. A NIST-certified ruler is used as a guide to generate segments approximately 10mm in longitudinal lengths. Segments are cleanly cleaved using disposable microtomy blades. The proximal end of the segment is marked with a tissue-marking pen. Gross visual and tactile observation allows quick evaluation of disease state: vessels are categorized as either healthy (soft, pliant, minimally occluded) or diseased (stiff, incompressible upon gentle pressure, visible occlusion). Resulting segments are then individually placed into welled trays containing phosphate buffered saline held at 4°C. Segments are numbered depending upon proximity to the coronary ostia and labeled with the tentative disease status.

2.3. DESIGN, PILOT VALIDATION, AND IMPLEMENTATION OF A BENCHTOP APPARTUS FOR UNIAXIAL, LONGITUDINAL, NON-DESTRUCTIVE MECHANICAL TESTING ON CORONARY ARTERIAL SEGMENTS

Longitudinal mechanical evaluation of intact coronary vessels is underrepresented within the published literature space. A majority of studies focus upon radial and circumferential stresses exerted by pulsatile blood flow, however the contractile motion of the myocardium tugs on components connected to coronary

arteries and generates non-negligible longitudinal forces. To further elucidate the mechanical response, a custom apparatus for benchtop testing of healthy and diseased coronary arterial segments was developed to recreate the actions exerted in vivo. In order to thoroughly interrogate the vessel wall, force or displacement must be evenly conveyed through the whole of the vessel wall. Even conveyance is hinged upon a thorough but non-destructive connect between sample and apparatus; it is crucial the attachment itself does not introduce artifacts during testing.

For the initial design, two criteria were laid out. 1) Attachment of the sample to the apparatus should be non-destructive, that is the native geometry of the vessel should be minimally manipulated during attachment. 2) The probe tip had to facilitate uniaxial application of force or displacement to the attached tissue. 3)Testing of the vessel must be non-destructive as histology must be performed downstream. These restrictions guided the additional developments made to the design as detailed in the following sections.

2.3.1. Development of a Mechanical Probe for Non-Destructive Sample Mounting

A brief literature dive revealed two general strategies for mounting vessels: Method I begins with a single cut placed along the long axis of the vessel, the vessel can then be flattened to create a planar sheet. Attachment to the setup is achieved through the use of hooks, grippers, or gritted paper. Although a planar sample is much easier to attach, resection of the tissue creates a mechanical defect within the axis of interrogation. Method II flattens the intact vessel into a plane at either end of the sample, attachment is then performed like in method I via hooks, grippers, or gritted paper. Neither strategy maintains the native geometry of the vessel.

To meet the criteria described previously, a smooth, spherical probe tip was proposed as the interface to the vessel. Following insertion of the probe, the vessel could be lightly cinched down around the mounted sphere. The rounded surface would allow applied forces to be conveyed tangentially at the interface and through to the remainder of the vessel. Cinching the vessel down mean the apparatus would interface across the whole of the vessel wall on both the interior and exterior surfaces.

The mechanical probe needed to be stiffer than the expected majority of tissue components in order to ensure the sample would yield before the system. The majority of plastics and rubbers were ruled out for the sake of simplicity leaving glass and metal as potential materials. Chemistry-grade borosilicate glass was explored as a material as thinner rods could be readily fired polished using an acetylene torch. The resulting glass probes would be highly biocompatible in comparison to metal, however centering of a glass bulb would be difficult given the equipment limitations within the laboratory. As such, metal was chosen as the material.

Initially, custom machined steel probes were proposed, however limitations in equipment and materials excluded this option. Untreated aluminum substrate was readily available however exposure to biological materials (namely salts) would create unwanted reactions on both the sample and the probe. With these restrictions in mind ready-made materials were employed in the development of the probe. Stainless steel, flat-headed sewing pins were chosen as the interface between the probe tip and the remainder of the mechanical set up. Mass manufacturing standards meant the pin diameters were consistently thin enough to be inserted into a set screw for ready connection to the remainder of the apparatus. Various adhesives were considered however to maintain probe integrity it was decided the probe composition remain wholly metal, as such solder was selected to bond the components. The needle tip of the stainless steel pins were neatly trimmed. The regions to be soldered were then lightly sanded to promote bonding and rinsed in methanol to remove debris. The trimmed region of the steel pin was inserted into the set screw, the overall probe centered using a tapped block to hold the screw itself and forceps to hold the pin. A fine tipped iron was used to perform the soldering, then the construct was allowed to cool.

Given the wide range in vessel diameters, different rounded probe diameters were desirable. Rounded metal beads and ball joints were explored however their acquisition and processing would prove exponentially difficult given their sizes. Instead, to achieve both custom sizing and shaping, solder was manipulated to form the desired rounded surfaces.

The flat-headed end of the pin served as a natural bulk point for further adherence of solder. Unsheathed stranded wire was wrapped around the pin shaft just beneath the pin head to enhance adherence. Solder was then applied using a fine tipped iron and shaped into a rounded surface. After the probe construct was cooled, the probe was unscrewed from the holding block and placed into a methanol bath overnight to remove unwanted rosin, further ensuring that attachment was due to solder bonding and not rosin adhesion. Loose probe connections were resoldered until solid bonding connectivity was ensured.

During mechanical testing, the tissue was continuously hydrated using saline. Probes were routinely cleaned and disinfected following use via rinsing in DI water, then an overnight soak in enzymatic (MetriZyme). Though the stainless portion proved robust, the spherical tip would inevitably show exposure fatigue however this proved a minor deterrence as the probe could be easily renewed by simply removing and soldering on a new sphere. As such, a custom probe tip was developed that maintained the native open, circular geometry of the vessel while facilitating thorough attachment across the whole vessel wall.

2.3.2. Development and Implementation of a Method for Delivering Even Longitudinal Force Along the Entirety of the Vessel Segment

The previous section detailed the development of the probe tip for adequate sample attachment at one of the vessel segment. Uniform delivery of force however, requires attachment at both ends of the specimen. The former construct was used to anchor the specimen to mechanical ground; we initially proposed that the other end of the vessel mirror the first. However, it became necessary to consider the larger apparatus when considering motion.

To aid in uniaxial motion, the larger apparatus used optical cage and rod components (ThorLabs Inc) to ensure alignment. Briefly, a 60mm cage cube (LC6W, ThorLabs Inc) was used to establish the primary axes of the apparatus. Caged rods were used to extend the axes to allow the incorporation of other compatible mounts.

Use of rods prevented off axis motion; the probe described before was further mounted into a tapped optical post which was itself, mounted onto a custom-machined aluminum disc. The use of an aluminum disc was critical as the disc could be loaded into a compatible cage plate and readily relocated along the cage axes. (see figure 1 below). The cage rods are finely machined to facilitate motion of components but are ultimately geared towards fixations of components; not meant to be used during controlled linear motions. A sliding cage system was proposed to incorporate the probes at both ends but design of such as system exceeded the scope and time frame of the project. As such, a compromise was achieved to develop a simplified method of applying uniaxial force precluding complex mechanical apparatus that could be suspect to hysteresis and failure points.

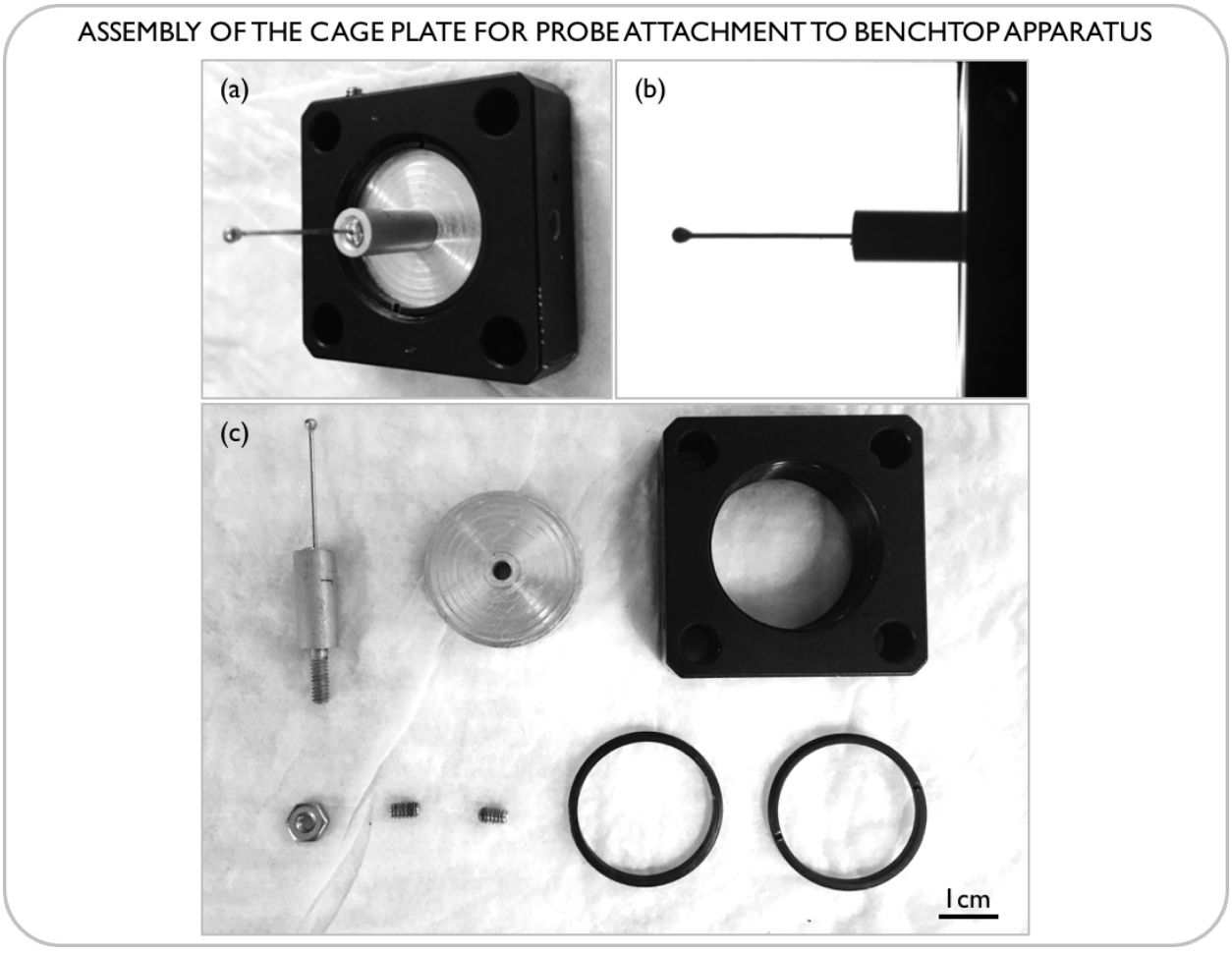

Figure 1. Assembly of the cage plate for probe attachment to benchtop apparatus. (a) The fully assembled optical cage plate housing the custom made probe. The probe has been soldered into a set screw; this construct is then screwed into an aluminum optical post holder and attached to a machined disc ~25.4mm in diameter allowing it to be firmly secured in the cage plate. **(b)** A view of the mounted tip backlit by the light pad. **(c)** The components of the cage plate. Disassembly is critical in cleaning and maintenance as the metal optical cage components occasionally come into contact with saline solution.

Samples are tied down with suture onto the test probes. The probe is inserted into the vessel lumen and the wall is then tied down onto the stainless steel shaft; the force is ultimate conveyed through the whole vessel wall however the attachment is grossly condensed to a point. In light of this, for the sake of simplicity we sutured down the opposing end to produce a similar condensed point. The remaining suture is then fed through a fixed pulley adjusted to allow relatively frictionless motion during application of force. To produce repetitive force applications, we used hooked laboratory scale calibration weights that could be ready placed and removed. The end of the suture line tied onto a rounded washer to prevent slack in the line. The washer (3.33g) also doubled as a convenient location for attaching the hooked weights.

2.3.3. Development of a Method for Observing Displacement of a Macro-sized Tissue Sample

Observation of displacement in a macro-sized soft tissue challenging is difficult as deformation does not occur uniformly. Various methods for observing tissue deformation are implemented in literature however the macroscopic nature of our interrogation renders these methods too localized to be representative of the specimen response. During pilot testing of the apparatus we explored variants of these methods to evaluate tissue displacement most notably observation of a fiducial feature ie. a side branch, and external application of a mark as a fiducial marker. Both of these strategies suffered from similar setbacks, both features distort as force is applied to the tissue, it is difficult to establish how to quantify the net displacement when the profile of the feature changes before and during force application. Additionally, the markers only represent the deformation of the region they are local to. As an example, the displacement of a side branch only represents the deformations experienced by the side of the vessel it is located upon. Bearing in mind that the aim was to interrogate the whole of the vessel, it became necessary to develop another method for evaluating displacement.

Two criteria were established. First, if a marker was implemented it had to be relatively resistant to distortion. Two, the marker had to be representative of deformation within the whole vessel wall. Force is applied through the whole of the vessel wall via the suture line. Thus we proposed that an ideal location for the fiducial would be within the line of force itself ensuring that the net displacement within the line would

result from net tissue deformation. To produce a robust fiducial, several methods to place a small, stiff marker were made including use of paraffin wax and inclusion of a small bead. Pilot attempts revealed that the marker needed to be symmetric relative to the suture line as slight rotations in the line were observable under magnified observation. Excessive disruptions to the suture would also cause later failures, application of wax would cause local changes in suture stiffness and inclusion of a bead produced mechanical deficits (due to the roughness of the bead) in the suture leading to line snap failures. Following thorough exploration of these methods, it was found the simplest way to produce a robust, in-line marker was to simply tie a single knot in the line. As the suture was pre-stretched the resulting knot distorted minimally with application of force and was symmetric enough to minimize changes in profile in the event of slight rotations.

2.3.4. Refinement of Imaging Axis Incorporating Machine Vision Camera and Backlighting

Machine vision cameras possess the necessary resolution and framerate for observing the resulting motion from application of force. Preliminary work revealed that the average max displacement for the samples prior to sample tearing fell in the range of 1-1.5mm. Additionally, as the motion was uniaxial, this allowed adjustments to be made to minimize the necessary field of view (FOV). Restricting the FOV during machine imaging is critical as it allows increases in frame rate to occur. Prior to formal data collection it was not entirely clear how quickly changed in displacement would occur as such it was critical to maximize the possible frame rate in order to minimize the risk of undersampling the motion. A monochrome CMOS USB machine vision camera (EO-0413, Edmond Optics) was incorporated into the setup to observe the displacement of the fiduciary knot. Each sample had to be mounted and unmounted from the setup, thus to minimize the physical interference of the camera in the experimental space a vertical imaging setup was selected.

Additional rod and cage components were incorporated to facilitate alignment and prevent unwanted shifts and rotations within the set up. A fixed focus lens was employed and adjusted such that the desired FOV remained in focus. A NIST ruler was employed to determine the relative scale of the FOV. Below the imaging plane, a light pad was placed to enhance the contrast of the fiducial knot. Experimental frame rates

were dependent upon the size of the region of interest set during the acquisition process, all rates fell within the range of 120-150FPS.

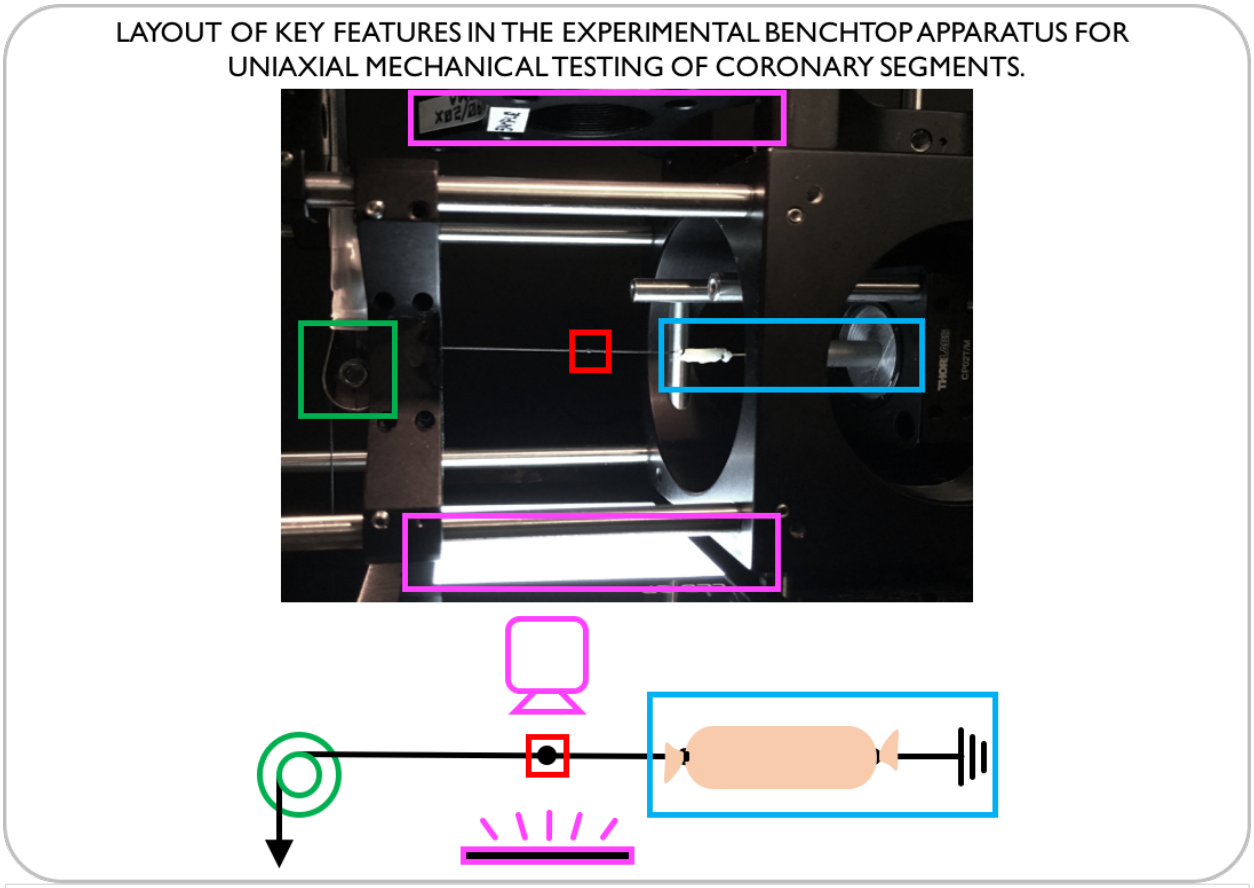

Figure 2. Layout of key features in the experimental benchtop apparatus for uniaxial mechanical testing of coronary segments. Starting from the right, the blue box indicates the position of the mounted coronary segment. A portion of the cage plate is visible representing the mechanical ground in the accompanying diagram. Suture is used to bind both ends of the coronary segment to the apparatus. The force delivery line is then knotted again to form a fiducial marker boxed in red. The displacement of this marker is observed by the optical system seen in magenta. A light pad below the marker enhances the contrast of the video taken by the machine vision camera above. All images used to determine tissue dimensions are also capture within this setup. Finally, the remainder of the suture line fed through a pulley, seen in green on the far left, and attached to a 3.4g washer (not shown). Camera perspective has skewed the path of the suture resulting in what appears to be an upward slope in the suture line; this is not present in the actual experimental set up as great care was taken to ensure the uniaxial delivery of force to the sample.

2.4. IMPLEMENTATION OF A CUSTOM BENCHTOP APPARATUS FOR UNIAXIAL MECHANICAL TESTING

Prior sections detail pilot development; this section focuses wholly on the experimental process used to collect data used to collect displacement data and the relevant vessel dimensions for Young's Modulus calculations (see figure 3 Below).

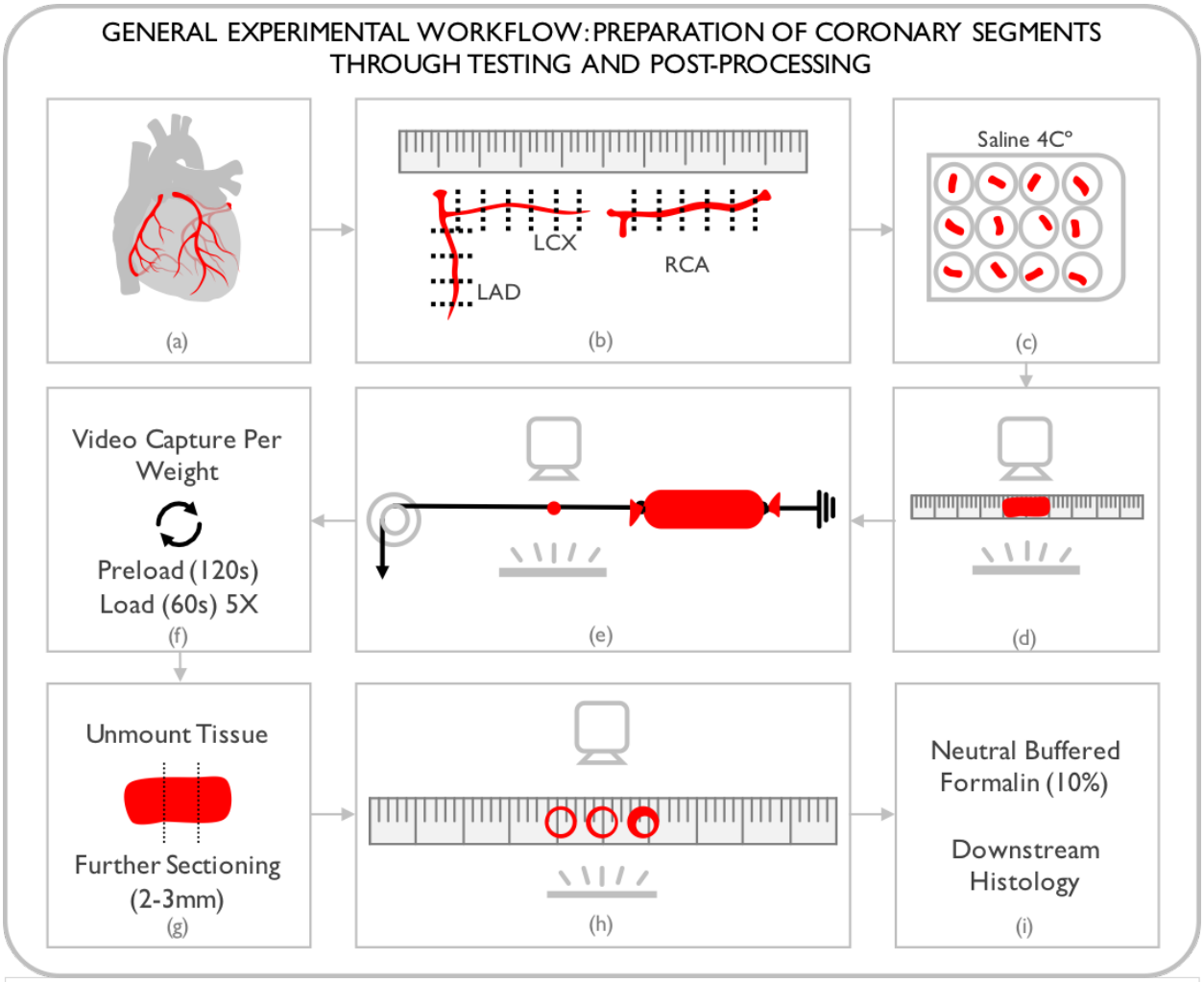

Figure 3. General experimental workflow spanning preparation of coronary segments through testing and post-processing. Regardless of sample source and accompanying serology, all tissue samples are treated as infectious. The coronary arteries are carefully extracted favoring the proximal portion where disease tends to manifest more severely. Excessive tissue is removed and samples are cut into 10mm segments and stored individually in welled trays filled with saline. An image is take of the intact vessel to determine initial length and outer diameter. (a-d) The coronary segment is then mounted onto the probe and the probe onto the caged apparatus. Suture is used to cinch down the opposing end before being knotted to form a fiducial marker and drawn through a fixed pulley to facilitate force delivery. Calibrated laboratory weights are applied for 120s to preload and 60s per experimental run; five runs are performed per weight. (e-f) The tissue is then carefully unmounted, further sectioned, and imaged again to determine cross-sectional area, inner, and outer diameter. Segments are then placed into 10% neutral buffered formalin for fixation prior to entry into the FFPE pathway. (g-i)

2.4.1. Coronary Segment Preparation and Probe Mounting

Following grossing and segmentation, arterial segments are kept individually in welled trays containing PBS held at 4°C. Under in-vivo conditions, arteries experience mechanical forces at 37°C however this is difficult to achieve in a benchtop research environment so all testing was performed at room temperature (60-65°F, ~20°C). To prevent temperature shifts from confounding the mechanical data, the current sample being interrogated was removed from the welled tray and placed in a room temperature PBS bath for 30min to allow temperature equilibration.

The physical parameters of the tissue were captured using the optical system prior to mounting. Coronary segments were gently blotted with a kimwipe then placed upon a NIST ruler and imaged; segment length and outer diameter were later determined during post-processing. The mechanical probe is then inserted into the lumen of the sample and the surrounding vessel sutured (2-0 silk ties) down using a single constrictor followed by a square knot on the opposing side. Excess suture is trimmed. The opposing end is then tied down in a similar fashion, however only the shorter suture arm is trimmed as the remaining line is used to deliver force through the sample. A single knot is placed in the remaining line, then the line threaded through the pulley and attached to the washer. The sample is hydrated using room temperature PBS throughout the experiment to prevent desiccation. This process was streamlined to take less than 5min in order to minimize sample exposure to air.

2.4.2. Preloading and Weight Application

Samples were interrogated at a maximum of five weights (three samples tore prematurely): 20g, 50g, 100g, 150g, and 200g. Following initiation of video capture in uEYE, weights were swiftly placed onto the washer in a controlled fashion. Weights were pre-loaded for 120s then removed. Five individual 60s runs were performed, weights were loaded and unloaded for each run. Samples were hydrated between runs using room temperature PBS however never during the run. Five experimental weights are used in total, each weight produces five recorded runs resulting in a total of 25 video runs for later analysis. This portion of the experimental run was streamlined to take less than 1hr to complete.

2.4.3. Unmounting and Post-Processing of the Coronary Segment

Following acquisition of the final video run, the artery is removed from the setup. First the suture line to the washer is severed such that the cage plate housing the mounted tissue can be removed from the remainder of the apparatus. Fine tipped forceps and microdissection scissors and scalpels are used to carefully remove the suture knots binding the opposing ends of arteries, effectively unmounting the tissue. Great care is taken to avoid producing cuts in the tissue during this process. The unmounted segments are then placed back into room temperature saline to facilitate rehydration for 10-15min.

Coronary segments are then further sectioned into 3-4mm long portions. The portions are placed axially upon a NIST certified ruler and imaged using the apparatus; post processing of this second image reveals the inner diameter and another measure of the outer diameter. Finally, these portions are placed into a labeled tube containing 10% Neutral Buffered Formalin and allowed to fix overnight under gentle agitation at room temperature prior to entering histologic processing.

2.5. SIGNAL CONDITIONING, PROCESSING, AND QUANTIFICATION OF VESSEL DISPLACEMENT USING CUSTOM IMAGEJ/FIJI AND MATLAB CODE

Videos resulting from uEYE capture are automatically saved in the AVI format; ideally the video data could be directly imported into MATLAB for analysis however incompatibilities between different operating systems necessitated an ImageJ/FIJI pre-processing step where imported AVIs are processed into image sequences and exported as TIFFs. These images are then loaded into MATLAB and the time course of the knot determined. Critically, the same MATLAB code also generates the max displacement

2.5.1. ImageJ/FIJI Pre-processing of Experimental Video Runs

FIJI (FIJI Is Just ImageJ, NIH) was used to process the experimental videos into image frames; it is worth noting that for our purposes, there is no distinction between ImageJ and FIJI but FIJI was chosen because of its increased utility due to pre-inclusion of the BioFormats module.

A custom macro was written to batch process videos. The macro would import an AVI file as an image sequence, rotate all images in the sequence by 90° such that motion proceeded from left to right, then export the image sequence as a series of serially named 8-bit TIFF images specifying the weight applied and which run out of five. Finally, the macro would output the total number of frames in each file and the frame rate, these data were collected into an Excel sheet.

2.5.2. MATLAB Determination of Knot Time Course Based Upon Intensity Profile Relative to Time

Initial analysis of knot displacement proved challenging, despite having a high contrast video of the knot motion image analysis programs do not know what the feature of interest is, as such a custom program had to be written. For this facet of the work, the high contrast provided by the light pad proved especially crucial as it improved identification of the knot profile and raised the signal-to-background ratio.

Tracking the whole of the knot as a discrete feature proved difficult as such a simplified method was developed to assess to knot profile as a distinct point. Import of an 8-bit TIFF image into MATLAB results in a matrix the with the dimensions of the image (in pixels) containing 8-bit intensity values. As knot motion proceeds uniaxially from left to right, summation of row values remain constant however summation of column values revealed shifting values corresponding to knot location.

Briefly, each image frame in the video was loaded into MATLAB, the image values were effectively inverted. Prior to inversion the knot appeared dark corresponding (ie. intensity values of 0-5), inversion renders the knot values bright (ie. intensity values 250-255) and the backlit background dark. Summation of columns forms a linear array of values where clustered peak values represent the knot location. The mean of these peak values above a user defined threshold is used as the knot location. This knot location is then saved into a matrix and the next image loaded.

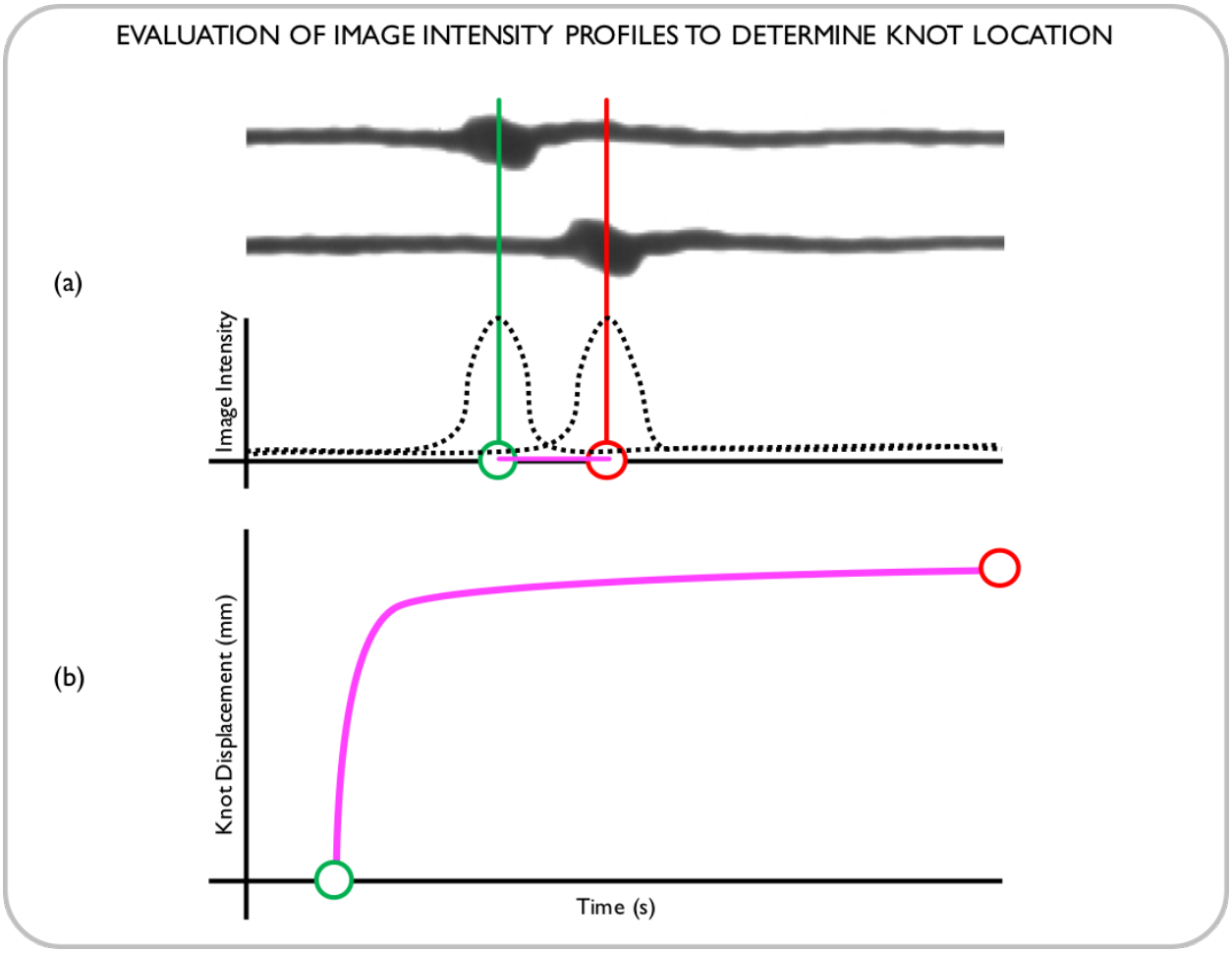

Figure 4. Evaluation of image intensity profiles to determine knot location. (a) Two representative video frames from an experimental run are shown. The top frame is the first frame prior to weight loading and the bottom frame the last frame captured during steady-state loading. Inversion and summation of image intensity values in MATLAB produces peaks centered around the knot position. A threshold value is selected, position values whose corresponding intensity fall above threshold are averaged to produce a single value representative of knot position. The green circle indicates the starting position of the knot, the red circle then final position. Magenta is used to represent the displacement. **(b)** When comparing only the initial and final frames only the net displacement can be determined, however knot position assessment is applied to all frames of the video, providing a view of the knot position with respect to time. This knot time course has been indicated in seen in magenta.

Processing of all image frames reveals the motion of the knot over time. Figure 4 above shows a diagram of this process. The location of the knot with respect to time is then exported as a text file. Finally, the max average max displacement of the knot is output and logged into an Excel file for Young's Modulus calculations.

2.5.3. IMAGE PROCESSING – QUANTIFICATION OF PHYSICAL VESSEL PARAMETERS

During the experimental process, images using the optical system of the apparatus in order to better determine the coronary physical dimensions. Images were imported into FIJI for scaled measurements. All shots included the presence of a NIST-certified ruler. ImageJ/FIJI incorporates tools that readily generate measured pixel values on imported images.

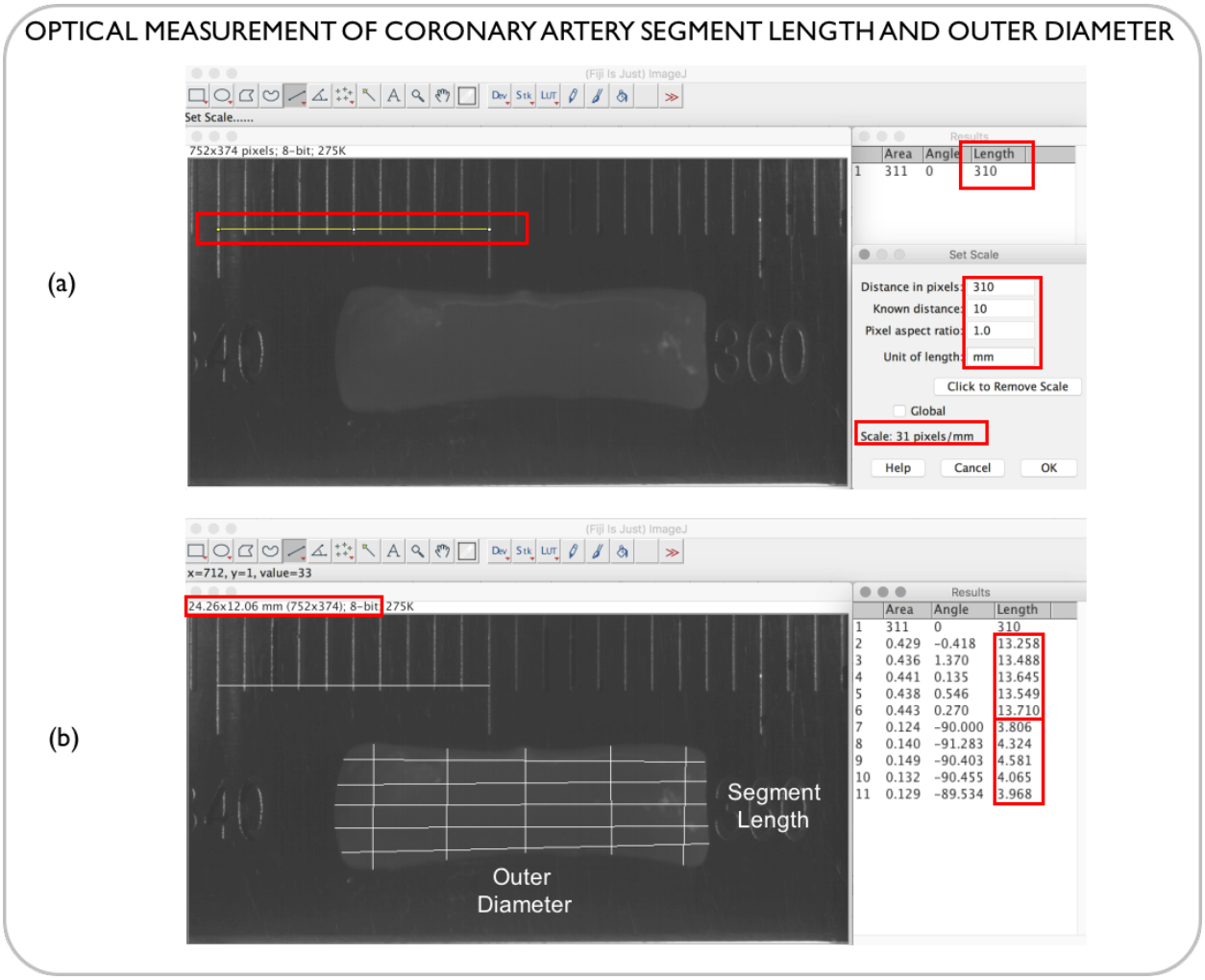

Figure 5. Optical measurement of coronary artery segment length and outer diameter. (a) Measurements are performed in ImageJ/FIJI by importing the image taken of the segment during experimentation. A NIST-certified ruler can be see in the background behind the vessel segment. In the upper left, a red box has been placed around the line tool highlight which spans a physical distance of 10mm. Performing a measurement reveals the highlighted line is 310 pixels in length allowing the scale to be set in the lower right. **(b)** Following scaling, measurements can be easily made using the same line tool. Note that the upper left now shows the scaled dimensions of the image. The measured regions have been manually filled with white to indicate where the measurements were made. Five length measurements followed by five outer diameter measurements are made. Note that the values produced are in mm due to scaling.

Drawing a line and performing a measurement generates a pixel length corresponding to the drawn line. A physical measure can be assigned to this pixel length: by drawing a line between two notches on the NIST ruler a pixel-to-mm scale value can be determined. Figures X1 and X2 describe the process for measuring the vessel dimensions needed to calculate Young's Modulus.

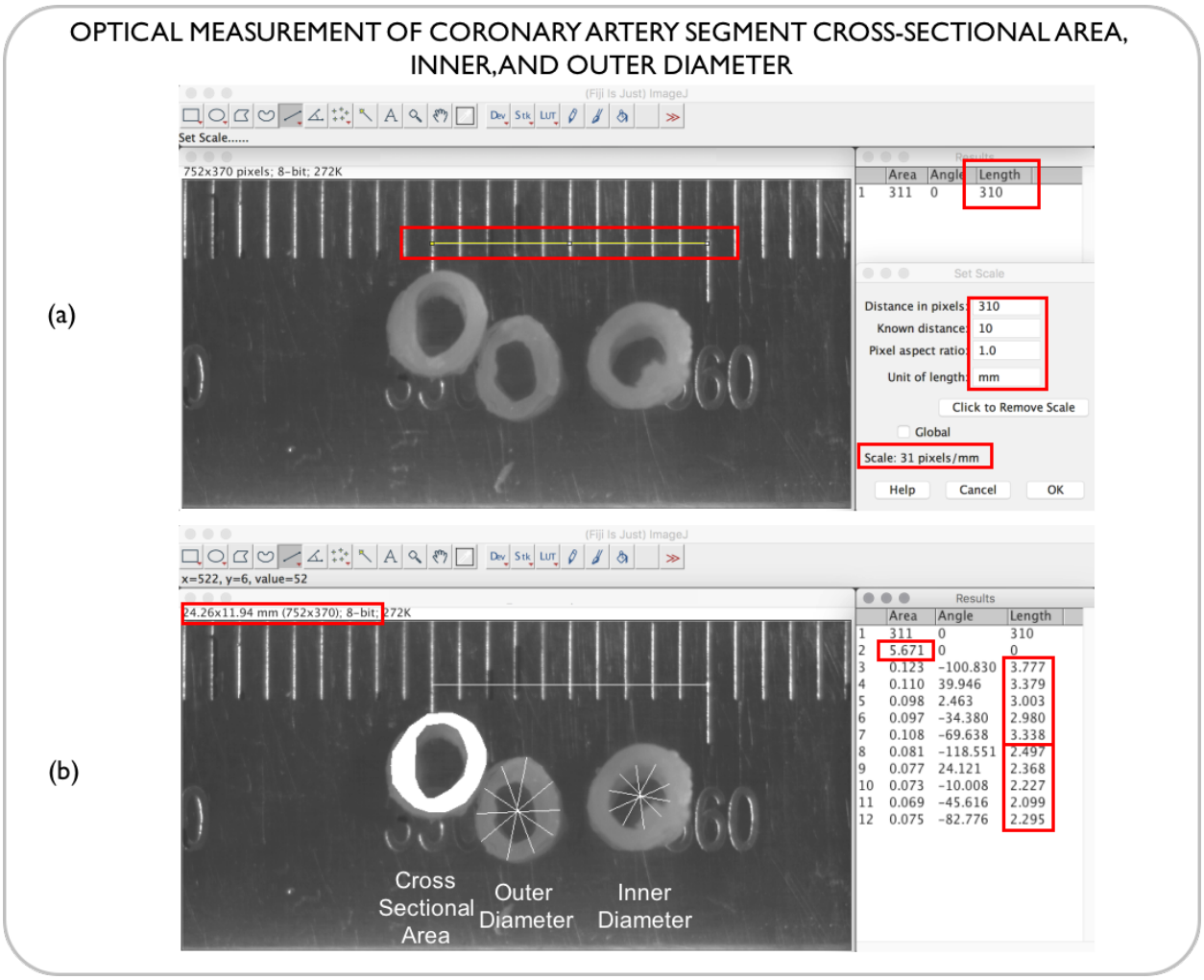

Figure 6. Optical measurement of coronary artery segment cross-sectional area, inner, and outer diameter. **(a)** Similar to the initial length and outer diameter measurements, following mechanical testing the segments are trimmed into smaller sections, placed axially, and imaged. The same scaling process is applied where a pixel measurement is scaled to a physical distance (see figure 5). **(b)** For each cross-sectional piece seen, the cross-sectional area, outer diameter, and inner diameter are acquired. For the sake of clarity, only representative measurements have been shown. For cross-sectional measurements, great care is taken so that tissue outside of the cross-sectional plane are not incorporated into the measurements.

After assigning the scale, measurements can be easily performed to determine coronary artery segment length, outer diameter, and inner diameter. For each physical parameter, five representative measurements were taken and averaged to best represent the sample dimensions. This is especially critical in assessing

diseased vessels as the inner and outer diameters can vary greatly even within a 10mm segment. Averaged physical dimensions are recorded into an Excel sheet and used for later calculations.

2.6. GENERATING KNOT TIME COURSE CURVES

The data for knot time course curves are generated during MATLAB image processing and analysis. (see figure 7 below).

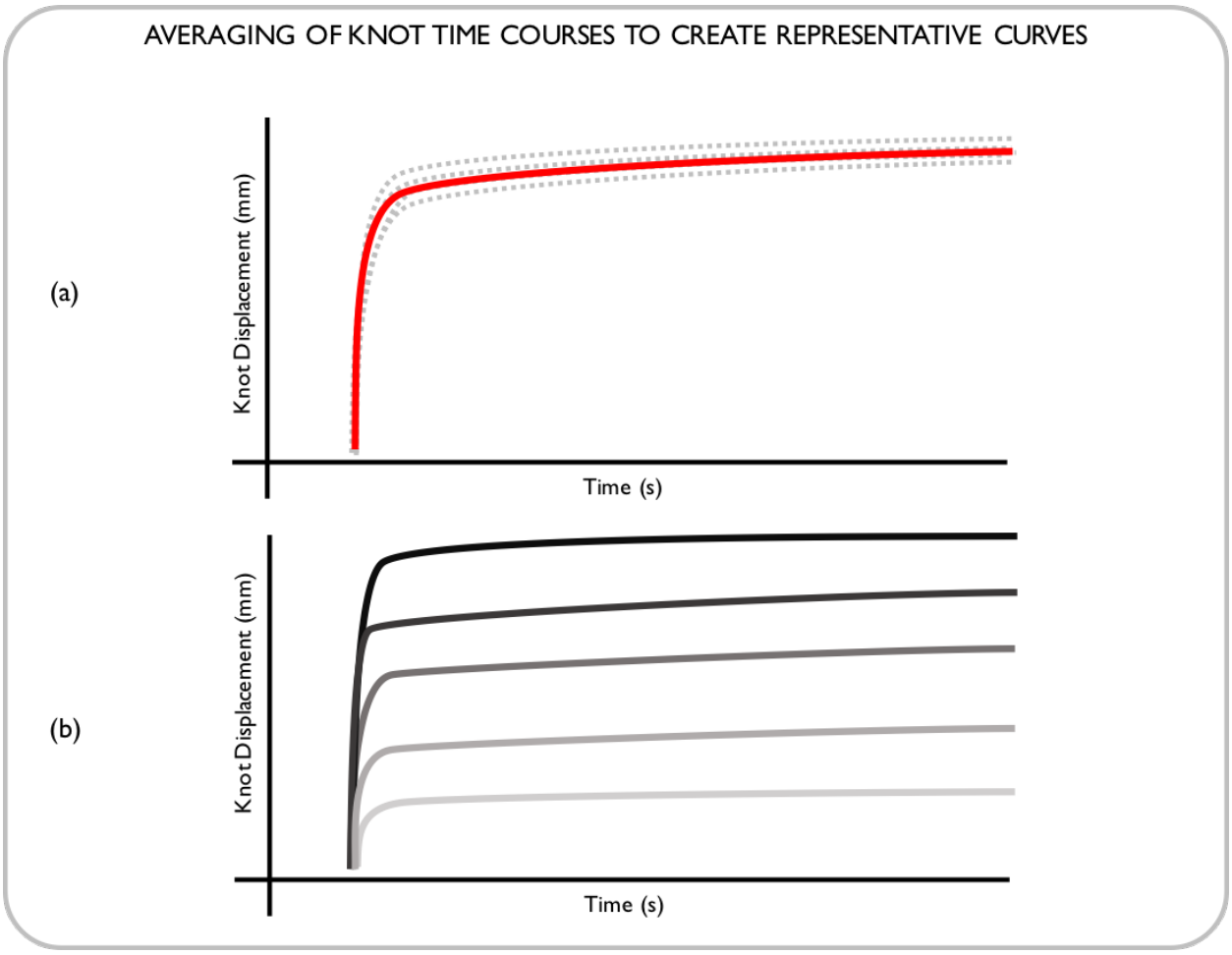

Figure 7. Averaging of knot time courses to create representative curves. (a) Weights are applied manually and experimental outcomes are subject to confounders whose control exceeds the scope of this project. As such, following preloading, five individual experimental runs are recorded generating five knot time courses. To eliminate spurious experimental errors, custom MATLAB code was written for temporal alignment and subsequent averaging of the curves. The averaged curves are shown as dotted lines in grey whereas the averaged curve is shown as a solid red line. **(b)** A total of five weights are applied, averaging of time courses produced five averaged curves representing those five weights. Here the trend from lighter to dark curves indicates an increase in weight.

Additional code was written to align and average curve motion to generate net curves. In short, the five repetitions performed per weight generated individual time knot time courses; these five curves are aligned and averaged to generate one representative curve. This results in five representative time course curves for each coronary segment, corresponding to the five different applied weights (20g, 50g, 100g, 150g, and 200g) as seen in figure 8 below.

2.7. GENERATING FORCE-DISPLACEMENT CURVES

The final steady-state max displacement values from the time course curves are used to generate force displacement curves.

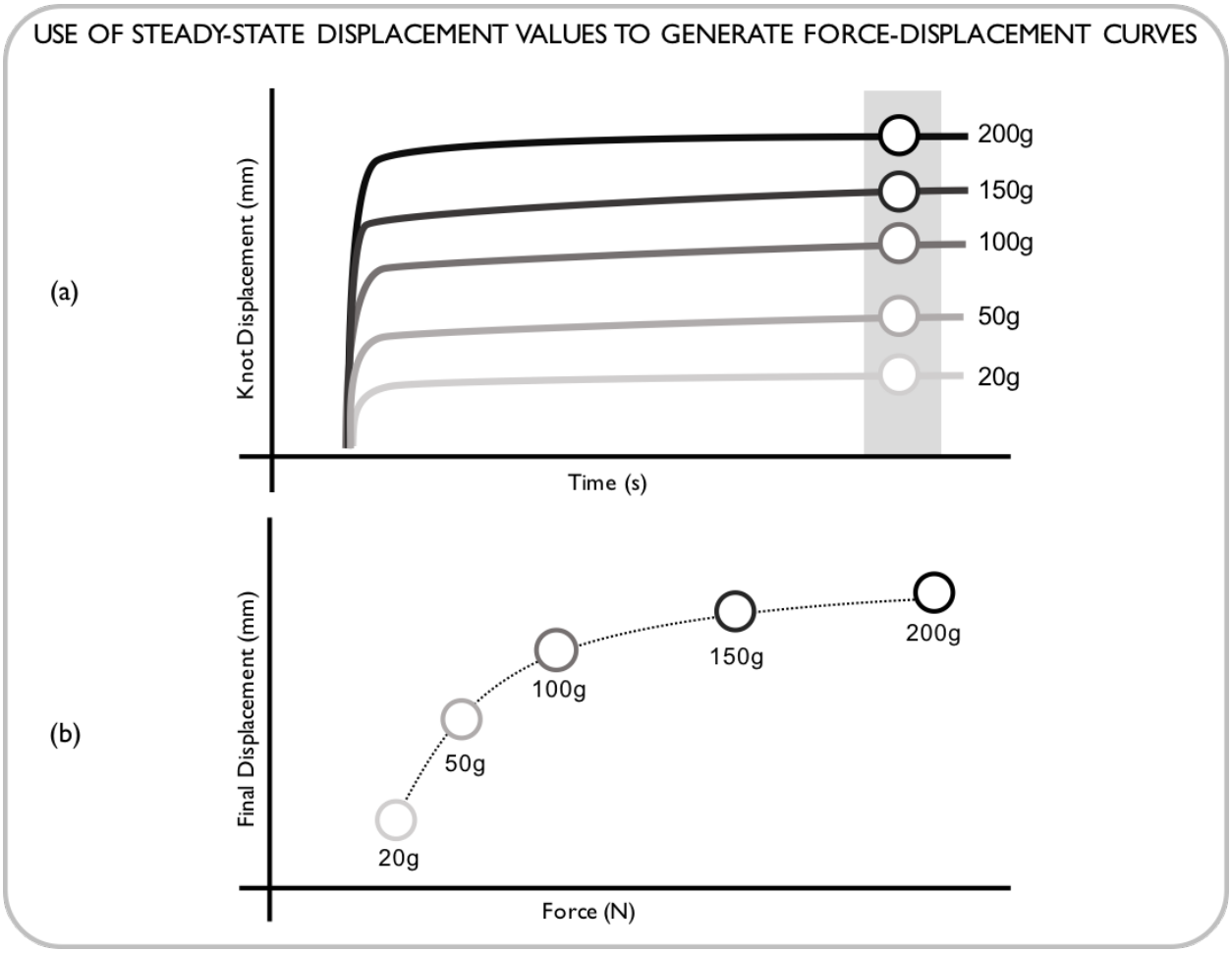

Figure 8. Use of steady-state displacement values to generate force-displacement curves. (a) A set of maximum steady state values are selected from the averaged time courses. MATLAB code is used to sort for the max values and averages the max 1000 values (arbitrary, approximately 10% of the total video frames) to generate the max displacement values. **(b)** These values are then plotted against calculated force to generate force-displacement curves.

Each tested segment was represented by a single curve comprised of five points representing the five different weights applied. Figure X above provides a diagram of this process.

Comparisons between different vessel categories were performed by performing point by point averaging. Segment disease status was previously evaluated via tactile feedback, binning segments as either healthy or heavily diseased. The curves of segments in these two groups were averaged and compared to one another. Similar comparisons were made between fresh vs frozen and human vs porcine.

2.8. GENERATING STRESS-STRAIN CURVES AND CALCULATING YOUNG'S MODULUS (E)

Force displacement curves provided some initial stiffness information on the coronary segments however these curves alone do not account for vessel geometry. Stress-strain values were calculated using the formula defined by Young's modulus (E).

$$\boldsymbol{E} \equiv \frac{stress}{strain} = \frac{\sigma}{\varepsilon} = \frac{\vec{F}/A}{\Delta l / L_0}$$

Values for force $\vec{\boldsymbol{F}}$ were calculated based off the known mass of the laboratory scale calibration weights. Initial length $\boldsymbol{L_0}$ was determined optically during ImageJ/FIJI measurements. Similarly, cross-sectional area $\boldsymbol{A}$ was calculated using the inner and outer diameter measurements taken in FIJI. Finally, the steady-state displacement values were used as displacement $\boldsymbol{\Delta l}$. For each coronary segment, a stress-strain curve was generated comprising of at most five points representing the different forces (masses) applied. Young's modulus (E) values were generated for each individual point within the curves.

2.11. HISTOLOGIC PROCESSING – PARAFFIN STEPS (CCVI)

Pathology remains the gold standard for diagnosis and analysis of tissue components. In pursuit of experimental rigor, a research histology laboratory was established at the Center for Cardiovascular Innovation. Protocols for formalin-fixed paraffin embedded (FFPE) and frozen sections were established based off input from clinicians and experienced histotechnicians. Ultimately, the lab aims to provide stains routinely performed during the clinical workflow but adapted to accept input of post-experimental tissue. The following subset of protocols has been adapted to provide additional analysis to further characterize mechanically tested vessels.

2.2.1. Grossing and Dissection – Post Mechanical Testing

As of this time, tissue entering the CCVI FFPE pathway results from two major experimental avenues, the cage imaging research and the mechanical testing research. As the primary focus of this document concerns mechanical testing, the grossing considerations for this work will be discussed at this time.

Prior to the initiation of the mechanical testing work, the coronary segments are already meticulously trimmed of excess adipose and connective tissue as their presence would confound tissue deformation. Concluding steps of the experiment require additional sectioning of the coronary segment into shorter (2-3mm) portions such that the samples can be laid flat and imaged to ascertain cross-sectional dimensions. Finally, these samples are placed into 10% neutral-buffered formalin (NBF) for overnight fixation.

2.2.2. Fixation and Decalcification

Coronary arterial segments are placed into 10% NBF within 8hrs of extraction from the housing tissue, with the resulting delay resulting from time allotted to processing and mechanical testing. Samples are fixed over night following a formalin change after the first hour of fixation. Decalcification is performed upon all human samples using a commercially available decalcifier system (Leica Biosystems). Lightly diseased samples are decalcified using a formalin-based decalcifier for 3-4hrs under gentle agitation at room temperature. Heavily diseased samples are treated with a stronger, hydrochloric acid based decalcifier for

15-20min under gentle agitation at room temperature. Following decalcification, all samples are thoroughly rinsed with PBS and reintroduced into NBF for subsequent processing.

2.2.3. Tissue Processing and Embedding

Samples are fixed for a maximum time of 24hrs prior to tissue processing and embedding. If needed, samples are transferred into 70% reagent alcohol for short term storage. Paraffin infiltration is accomplished with an enclosed, vacuum processor system (Leica ASP300S). Following infiltration, embedding is performed at 55°C (Leica HistoCore Arcadia H&C); arterial segments are oriented such that subsequent sectioning produces cross sectional cuts proceeding from the proximal to the distal end of the artery. Cooled blocks are trimmed and wrapped in foil for storage at room temperature.

2.2.4. Sectioning

A rotary microtome (Leica RM2255) is used to produce 6μm thin sections. Paraffin blocks are chilled upon a block of ice prior to sectioning. Ribbons are floated into a tissue bath containing deionized water at 45°C prior to separation and mounting upon a charged slide (Fisher Superfrost Plus). Paraffin slides are then angled to facilitate water drainage within a vacuum chamber prior to storage at room temperature.

2.2.5. Deparaffinization

Initial dewaxing is performed by placing paraffin slides into staining racks. The staining racks are then wrapped with foil and placed upright into a gravity convection oven at 60°C for 60min. Following heat-aided removal of wax bulk, the foil-wrapped racks are removed and allowed to cool briefly upon the benchtop (< 1min).

The slide-laden racks are removed and then subjected to a series of washes to passage the slides into water. It is worth noting that a d-limonene product (Clearene, Leica) is substituted for xylene as its deparaffinizing action is more gentle upon the tissue. Slides are ultimately passaged into deionized water and allowed to acclimate for no more than 10min prior to entering staining pathways.

2.4. HISTOLOGIC PROCESSING – MODFIED FFPE STAINING PROTOCOLS (CCVI)

In contrast to routine staining, these stains were performed singularly in order to distinctly isolate particular connective tissue component in anticipation of quantification during image analysis. Healthy and diseased slides were batch-processed together in an indiscriminate fashion to prevent bias.

2.4.1. Verhoeff-Van Gieson (VVG) Elastic Stain

The VVG stain demonstrates high affinity for elastic fibers and nuclei. VVG staining was accomplished by performing the first steps in the Russell-Movat Pentachrome staining protocol. Following rigorous differentiation, stains were passaged to d-limonene and mounted for subsequent drying and imaging.

2.4.2. Aniline Blue – Staining for Collagen

Aniline Blue is the stain responsible for identification of collagenous components during Masson's Trichrome staining. Following overnight treatment with Bouins, Aniline blue was applied for 15min and differentiated prior to passaging to limonene and cover glass mounting.

2.4.3. Evans Blue (EvB)

Evans Blue staining has been hypothesized to bind fibrous cap components. To better ascertain its specificities, EvB staining was performed on FFPE slides. Given that EvB is not a routinely applied histologic stain, a custom protocol was developed. Slides were passaged to water then placed in a 2% EvB bath housed at 60°C for 2hrs. Slides were then rinsed in tap water for 2min or until the water ran clear, then passaged through ethanol washes to d-limonene for mounting.

2.3.4. Cover Glass Application and Microscopy

Following staining of PPFE slides, all slides were passaged through alcohol washes into d-limonene (Clearene, LEICA). Mounting was accomplished with DPX mountant (DPX 13510). Following overnight drying, slides were cleaned and sealed. Briefly, the microscope construct consisted of an Axio Imager.A2 (Zeiss) upright frame with a mirror for dual brightfield and epifluorescence imaging. Brightfield imaging was accomplished using a 5Mpx color camera (Zeiss AxioCam 105; 0.5X adapter). Zen software (Zeiss) was

used to interface with the cameras. For routine image acquisition, standard Köhler transmission illumination was employed. Images were acquired at 2.5X or 5X for general acquisition, and at 10X if higher resolution of features were necessary.

2.4.5. Image Processing Prior to Analysis

Following image capture, files were exported as 24-bit RGB color TIFF files and stitched in ImageJ/FIJI (NIH) using the 'paste control' feature. Stitching of images is highly depend upon consistent imaging parameters, no additional adjustments except for minor focusing were made following initial white balancing and exposure. For quantitative work, shots were acquired at 2.5X to minimize the number of images needed to capture the entire section as stitching represents a potential source for artifacts. Stitched images are saved as a composite for subsequent analysis.

2.5. Quantification of Bright-Field Staining

Initially, routine application of stains was proposed to provide contrast however it was ruled out as all colors have contributing R, G, and B channel values during digitization. As such, although a stain may appear largely red or magenta to the human eye, during digitization it will invariably present with non-negligible G and B components. Color splitting could prove an interesting avenue for future analysis however for the scope of this research it was found that the simplest way to isolate the stain of the interest was simply to apply only the stain of interest.

All singularly stained slides were analyzed in the same fashion. Bright-field stains provide color by absorbing certain wavelengths, this is worth noting because unstained regions (including the tissue-less regions) appear white in color as there is no absorption or scattering. This similarity allows us to apply the rationale used during knot analysis; as such images were inverted such that the stained regions became bright and the unstained regions dark. The stains applied are routinely used in clinical histopathology given their specificity for certain features; proper application of the stain would show heavier staining in corroboration with more presence of a certain histologic feature.

A simple summation of intensity values would not reflect the differences in physical size of the vessels themselves as larger vessels would naturally contain more high intensity values than smaller vessels. To compare staining intensities intensity over a region would have to be considered, as such the mean intensity values were chosen as an initial point of comparison. Similar to the rationale for knot analysis, images were inverted such that the signal of interest became bright and the background dark. Mean intensities were then taken over the entire image and two local regions of interest to represent the staining intensity of the vessels.

CHAPTER 3: RESULTS

3.1. KNOT TIME COURSE COMPARISONS

In this section representative knot time courses are compared

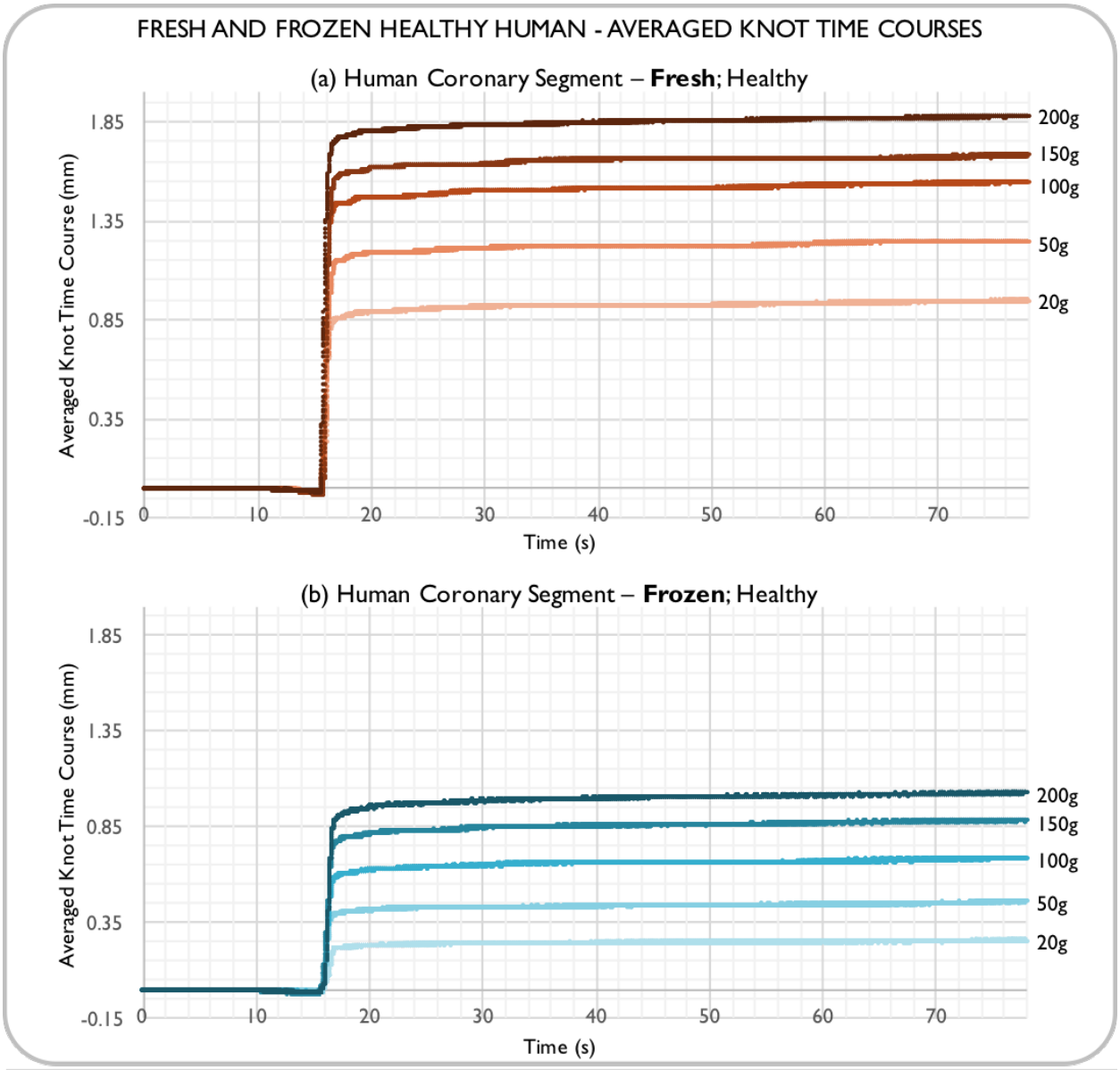

Figure 9. Comparison of averaged time courses for fresh and frozen healthy human coronary segments. (a) A representative example of an averaged time course for a healthy, non-frozen human coronary segment is shown **(b)** A corresponding example for a healthy, previously frozen human coronary segment. Observation of both traces show a near instantaneous displacement to the final length upon loading. Previously frozen healthy vessels displaced less than non-frozen vessels.

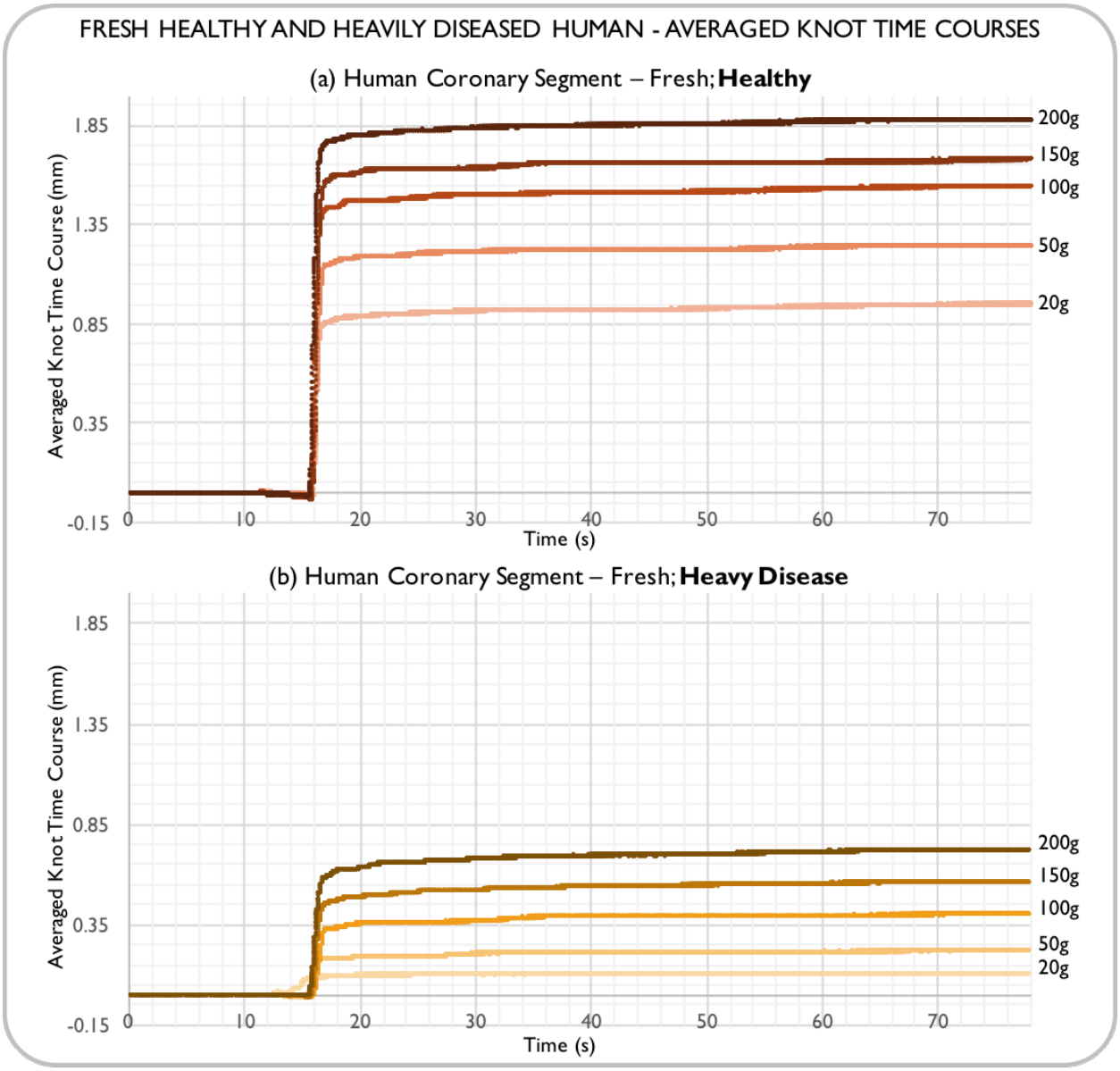

Figure 10. Comparison of averaged time courses for fresh healthy and heavily diseased human coronary segments. (a) A representative example of an averaged time course for a healthy, non-frozen human coronary segment is shown **(b)** The time course for a heavily-diseased, non-frozen human coronary segment is shown. Observation of both traces show a near instantaneous displacement however the diseased tissue appears to show a slight viscous component in comparison to the healthy segment. As expected, diseased vessel displace less than healthy vessels

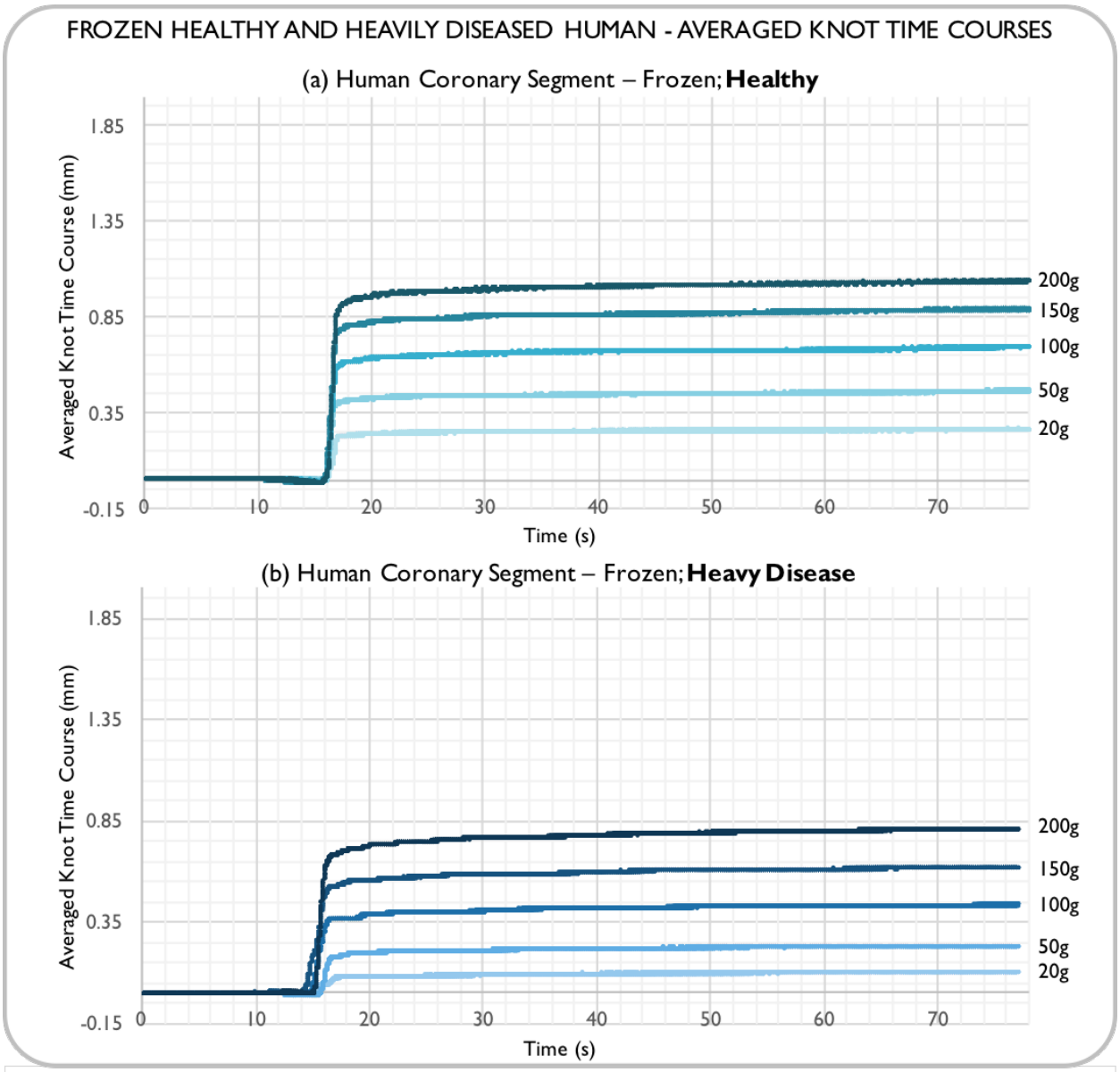

Figure 11. Comparison of averaged time courses for previously frozen healthy and heavily diseased human coronary segments. (a) A time course for a previously frozen healthy segment. **(b)** A time course for a previously frozen, heavily diseased human coronary segment. Both samples show limited displacement although the healthy segments do displace slightly more than the diseased segments

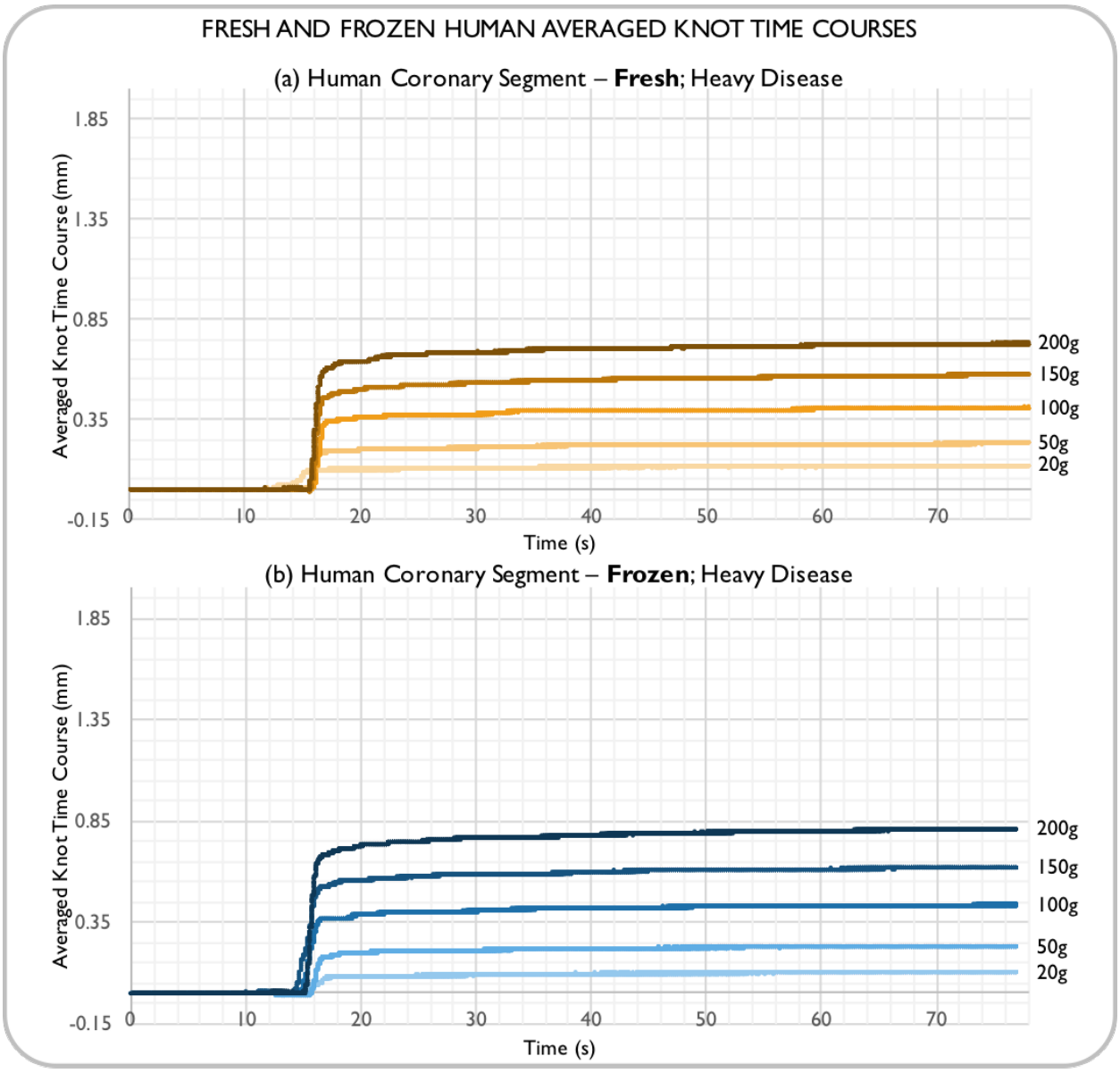

Figure 12. Comparison of averaged time courses for fresh and frozen healthy human coronary segments. (a) The time course of a non-frozen, heavily diseased coronary segment. **(b)** An example of a heavily diseased, previously frozen human coronary segment. Freezing causes a reduction in displacement in healthy vessels however this reduction is not observed in diseased vessel segments.

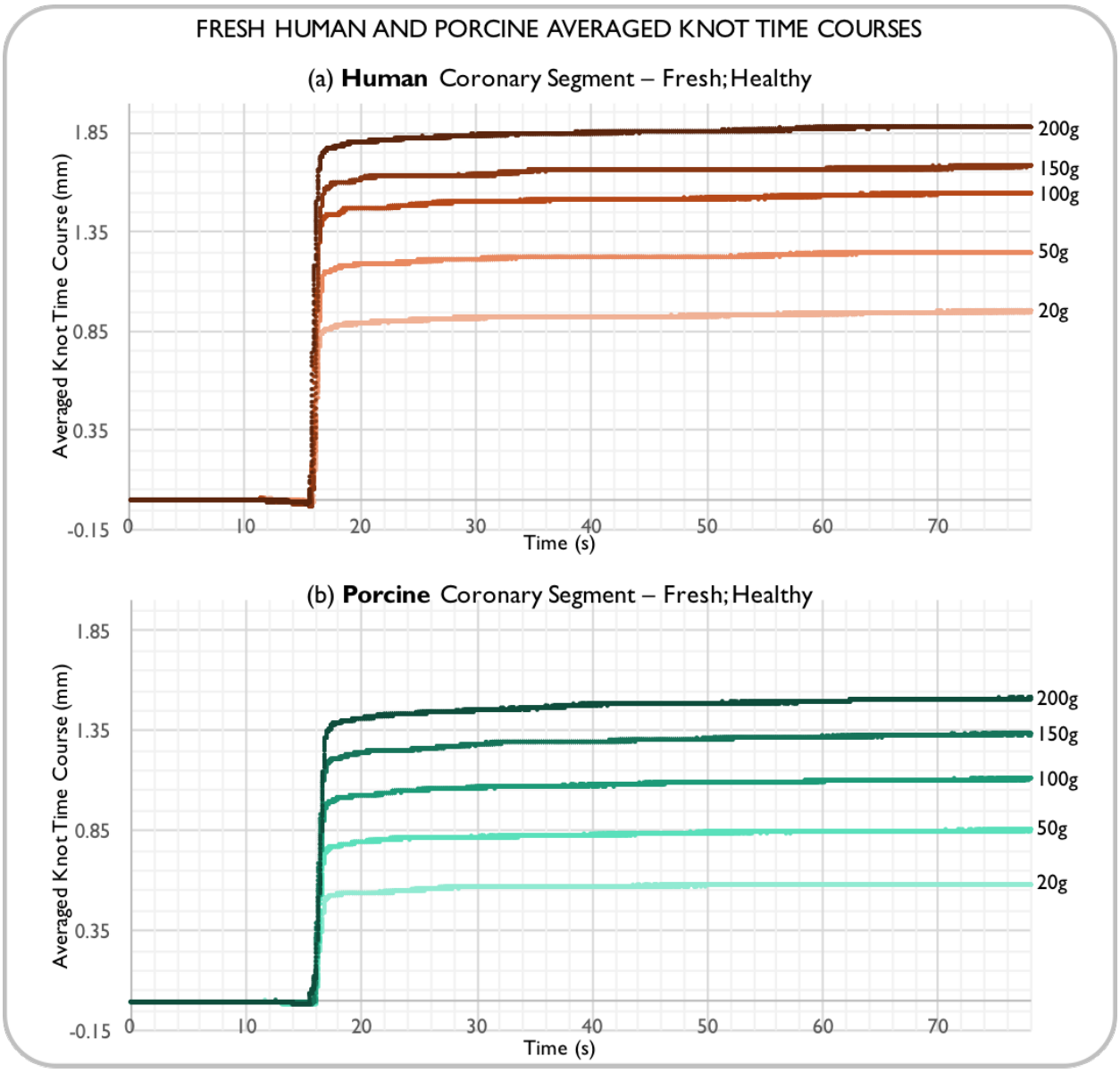

Figure 13. Comparison of averaged time courses for fresh human and porcine coronary segments. (a) Time courses for healthy, non-frozen human coronary segment. **(b)** Resulting time courses for healthy, non-frozen porcine segments. In this particular comparison the human traces displaced further than the porcine however as an overall population, the displacement traces are extremely similar to one another.

3.2. AVERAGED FORCE-DISPLACEMENT COMPARISONS

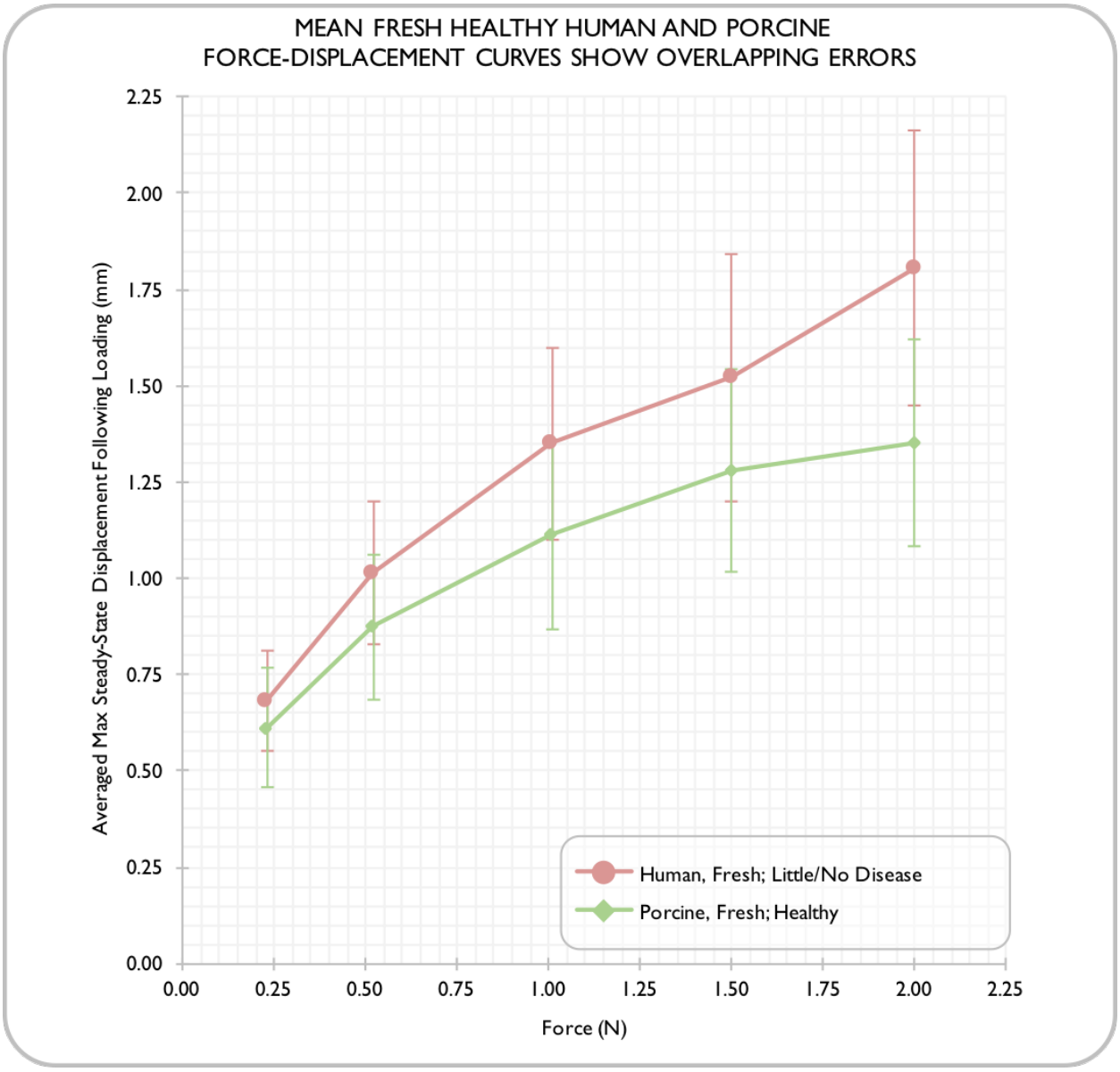

Figure 14. Mean net displacement curves for human and porcine segments show overlapping errors. The force-displacement responses of healthy human and porcine arteries are very similar. (Human, Healthy n = 8, Porcine n = 5)

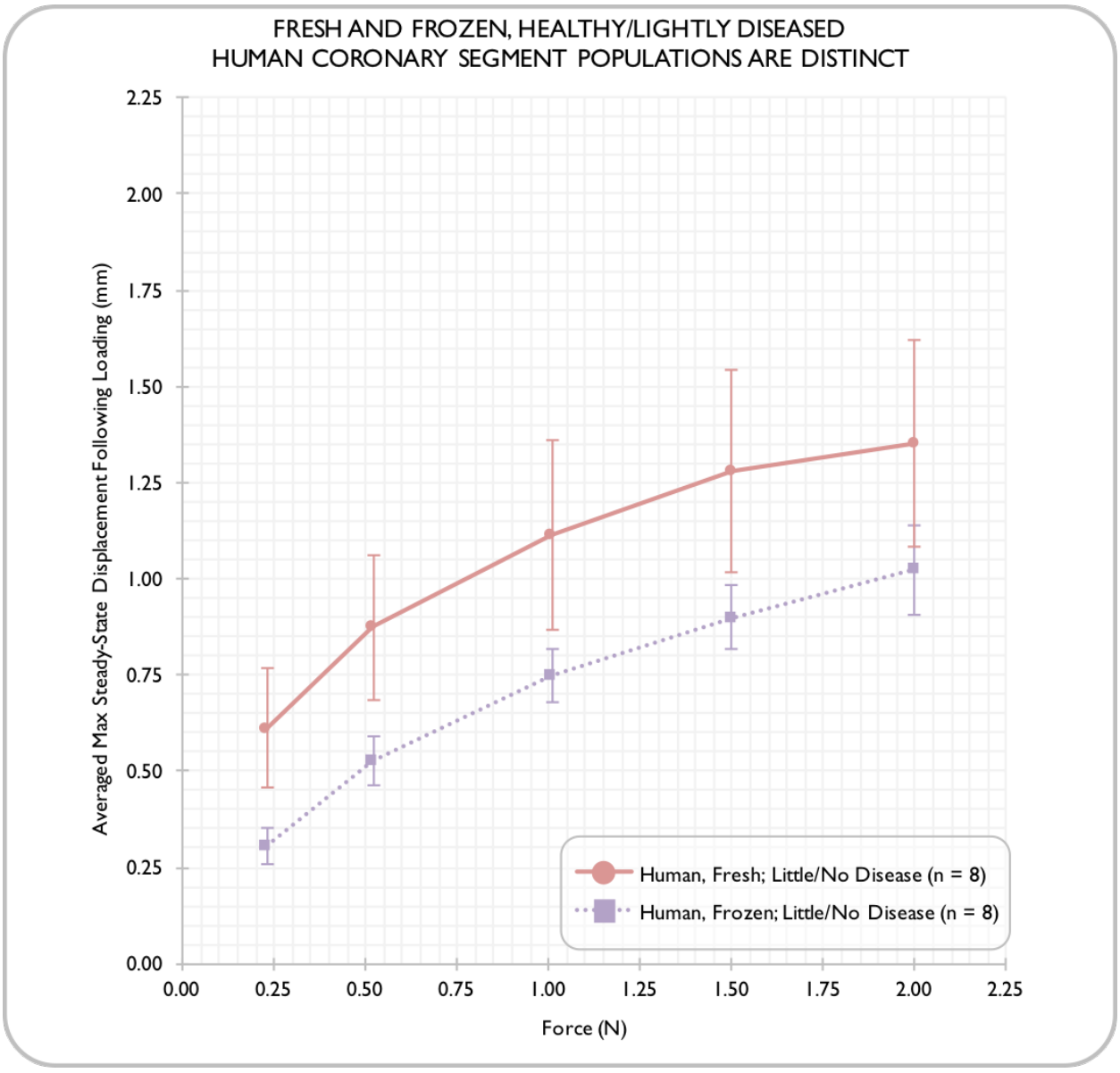

Figure 15. Mean net displacement curves for fresh and frozen healthy human coronary segments suggest they are distinct populations The resulting errors for these two groups do not show overlap suggesting they do not belong to the same population. (Human, Healthy Fresh n = 8, Human Healthy Frozen n = 8)

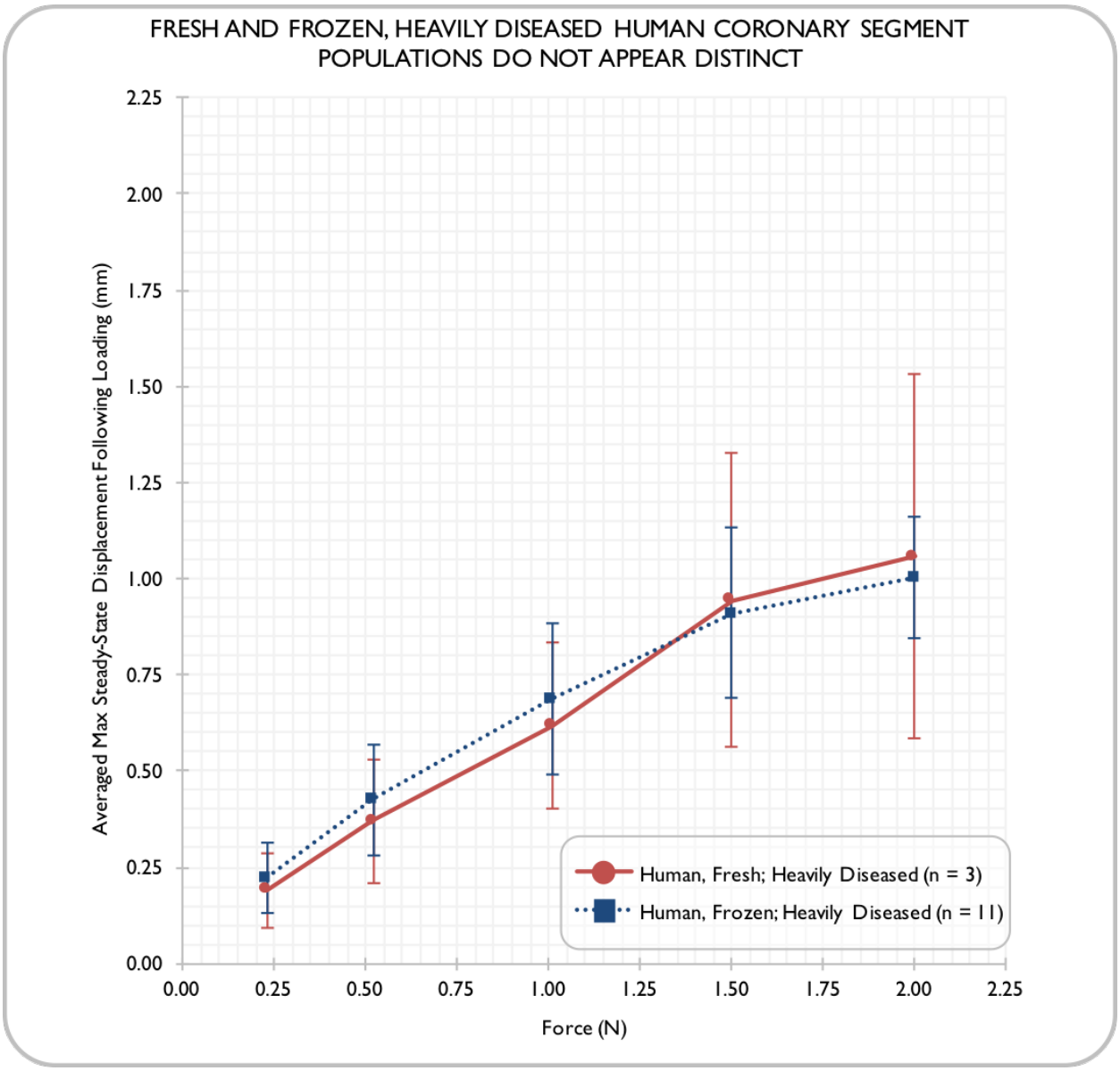

Figure 16. Mean net displacement curves for fresh and frozen heavily diseased human coronary segments suggest they belong to the same population. Similar to observations made in the time course comparisons, freezing does not seem to affect heavily diseased coronary segments in the way it affects healthy segments. (Human, Fresh Heavily Diseased n = 3, Human Frozen Heavily Diseased n = 11)

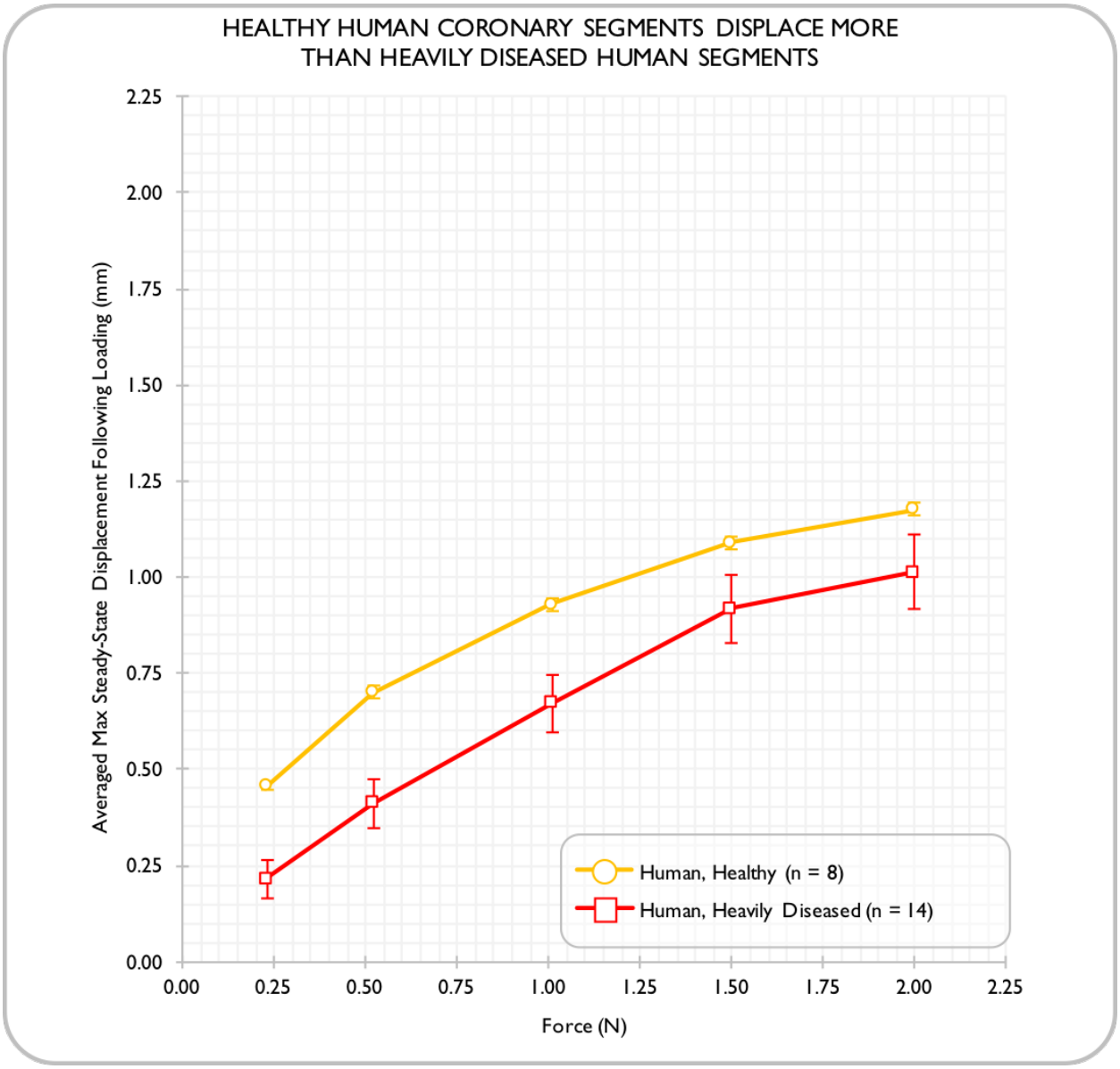

Figure 17. Healthy human coronary segments displace more than heavily diseased human segments. For this comparison, standard error of the mean was used as great rigor was applied in the experimental process and we can expect that these results reflect the true displacement values for these distinct populations. As freezing does not seem to affect displacement the frozen and fresh diseased vessels were combined. This comparison shows that healthy vessels displace more than heavily diseased vessel when loaded with the same weight, this is in support of hypothesis 1.

3.3. IMAGING AND QUANTIFICATION OF STAINED TISSUE

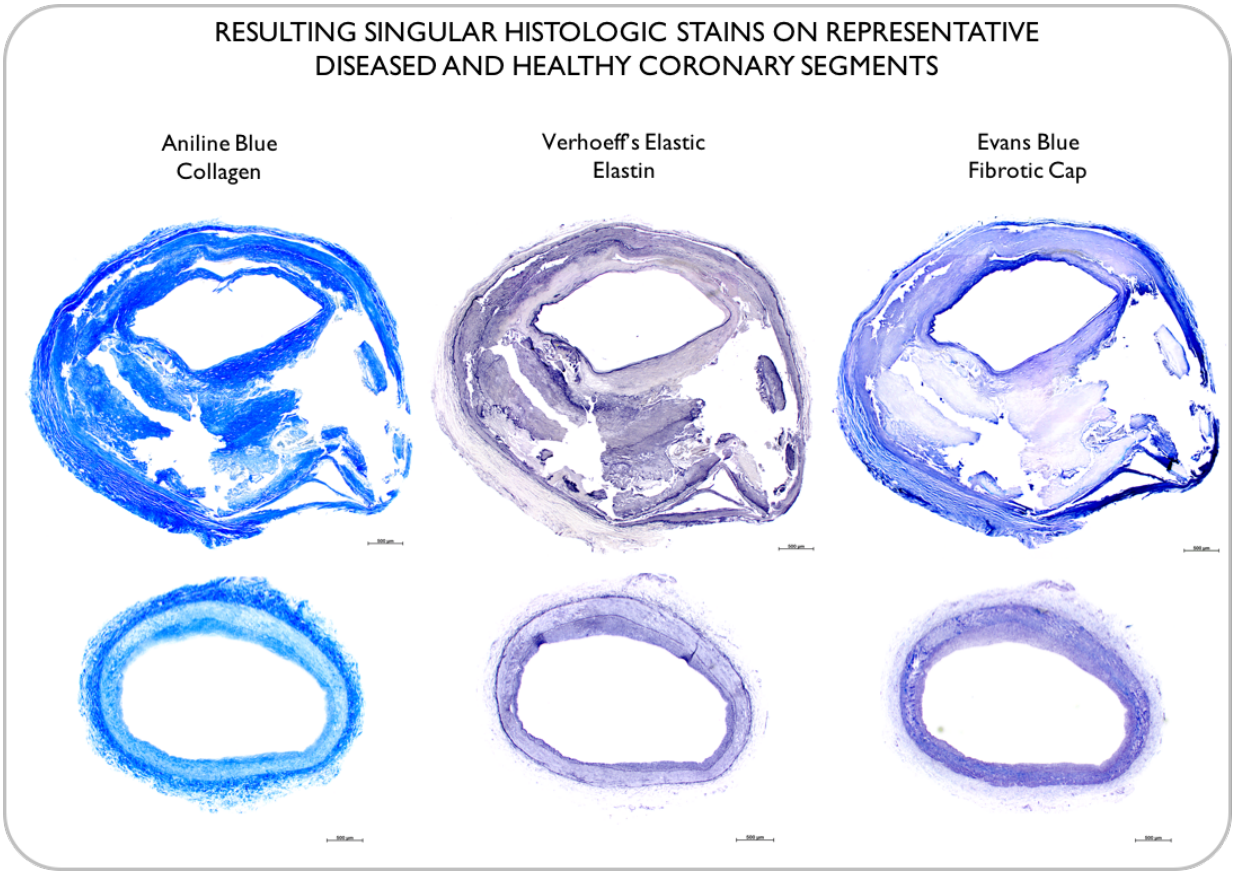

Figure 18. A panel of singular stains demonstrating the staining patterns of Aniline Blue, Verhoeff's Elastic stain, and Evans Blue. In comparing the staining patterns, Evans blue staining more closely matches that of Verhoeff's elastic stain for elastin than Aniline blue staining for collagen.

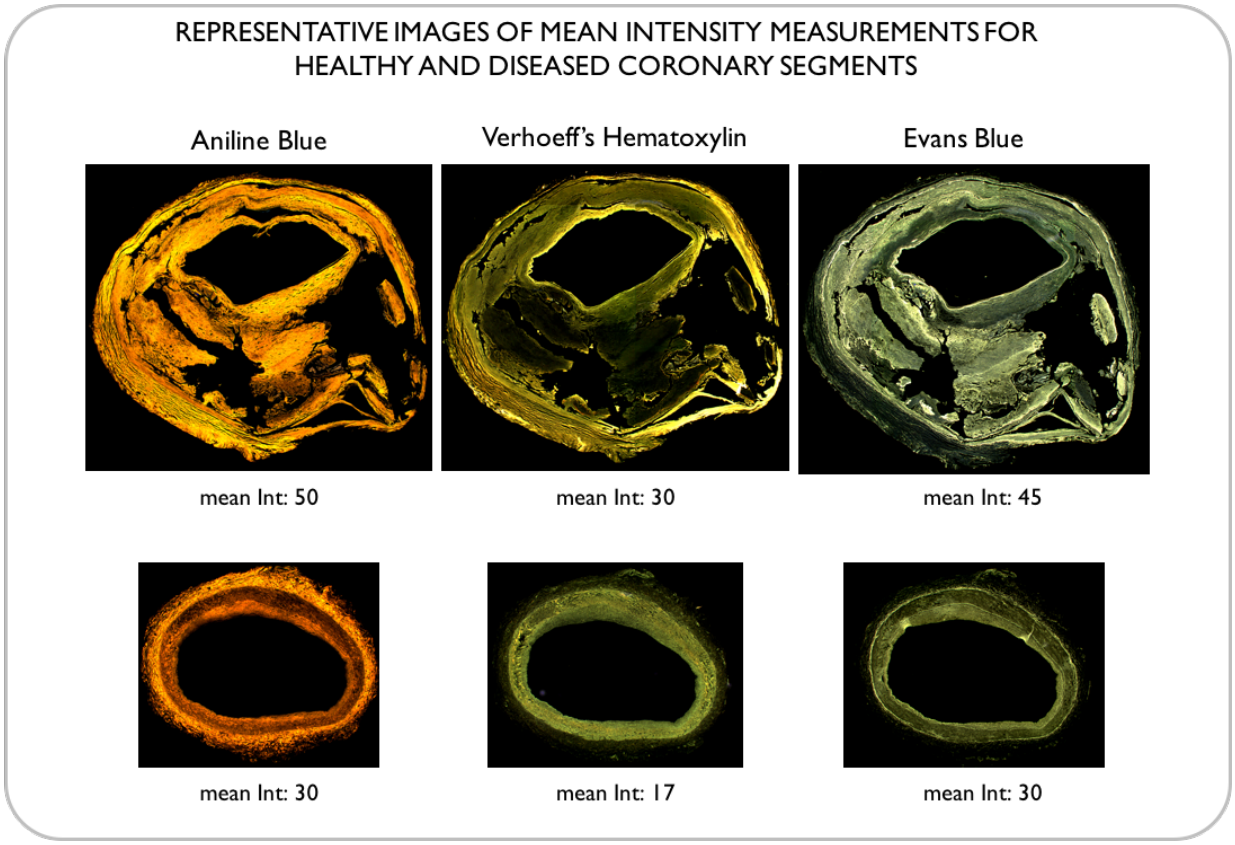

Figure 19. A demonstration of mean quantification of signal intensity over the entire image. Even in this generalized assessment, staining intensities for fibrous cap components were elevated in diseased vessels in comparison to healthy human segments. This is in support of hypothesis 2.

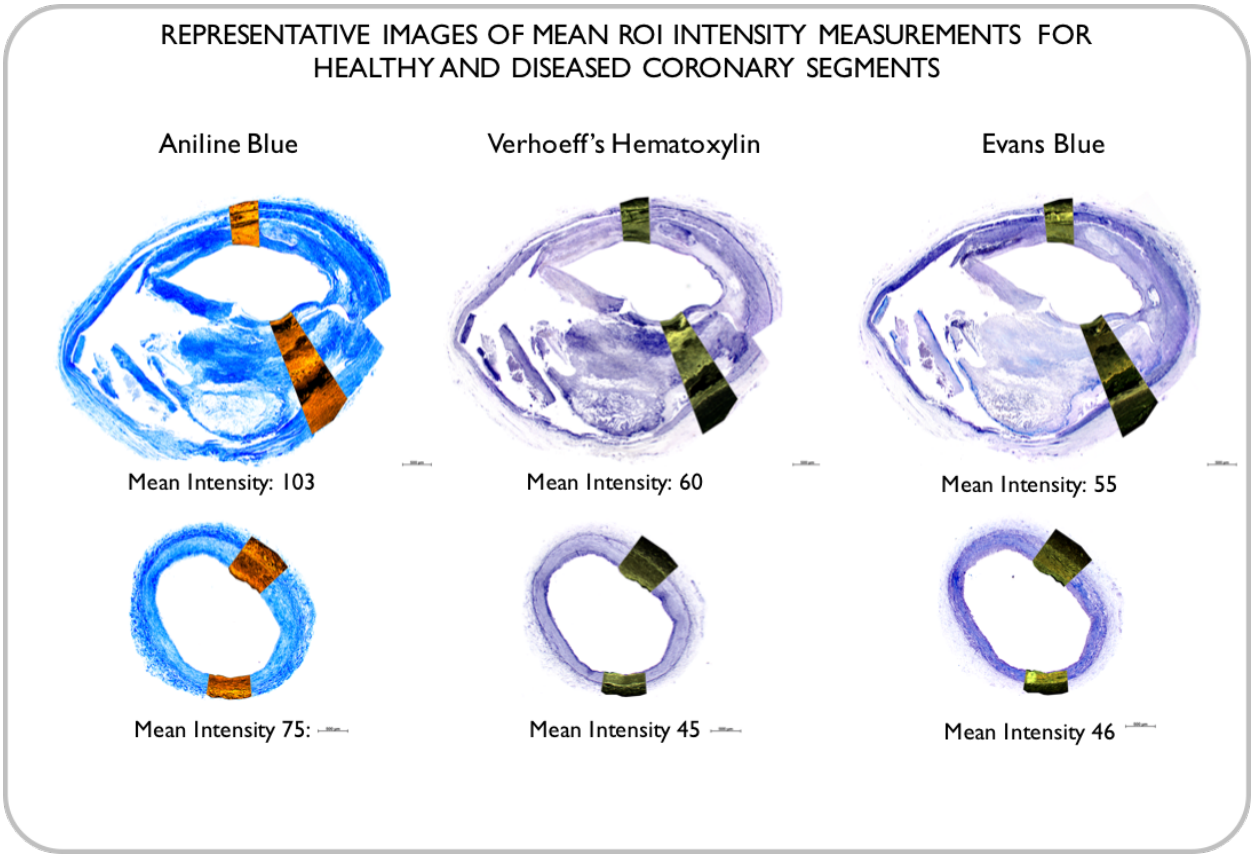

Figure 20. A more refined method of quantifying stain intensity focused upon regions upon isolated regions of interest. Similar to the mean intensity comparison, staining of diseased vessels was more intense than in healthy vessels, these data are in support of hypothesis 2.

CHAPTER 4. DISCUSSION

In brief, a custom mechanical apparatus was designed in order to perform uniaxial, longitudinal mechanical testing on coronary segments. This work was performed in order to investigate the following hypotheses:

Hypothesis 1: Diseased arteries have increased stiffness in comparison to normal arteries

Hypothesis 2: Evans Blue staining intensity will be higher in more diseased, stiffer vessels in comparison to normal arteries

Constraints mandate that the remainder of this discussion be completed in journal publications pending adjustments to the testing apparatus in order to ensure stress matching to ensure that Young's modulus comparisons can be made. Further histology will be pursued in order to improve the estimation made by the image quantification data. Finally, an improved thresholding algorithm will be applied to improve the specificity of the image quantification work.